Defect Generation in Layered Double Hydroxide Nanostructures for Water Splitting

By

Muhammad Abubakar Rana

School of Chemical and Materials Engineering

National University of Sciences and Technology

2022

Defect Generation in Layered Double Hydroxide Nanostructures for Water Splitting

Muhammad Abubakar Rana

Reg No: 00000275267

This thesis is submitted as the fulfillment of the requirements for the degree of

MS (Nanoscience & Engineering)

Supervisor: Dr. Amna Safdar

School of Chemical and Materials Engineering (SCME)

National University of Sciences and Technology (NUST)

H-12 Islamabad, Pakistan.

August, 2022

DEDICATIONS

Dedicated to my beloved parents who are unparalleled in the entire world and my siblings.

Acknowledgements

Allah Subhana-Watala, I praise You for guiding me through each stage of this project and for the countless brilliant ideas you planted in my thoughts. Without Your invaluable assistance, I would not have been successful. Whether it was my parents or any other person, whoever helped me with my thesis was doing Your will and deserves no praise.

I owe so much to my wonderful parents, who took care of me from the time I was a helpless infant until I was an adult and who have always been there for me, no matter what.

In addition, I'd like to thank my MS Research Advisor, Dr. Amna Safdar, and my MS Research Co-Advisor, Dr. Mashkoor Ahmad, for all their support and guidance. There is no one else from whom I have learnt about engineering topics as thoroughly as she has.

Dr. Zakir Hussain & Dr. Muhammad Siyar, who served as members of my thesis guidance and evaluation committee, also have my deepest gratitude. Additionally, I owe a debt of gratitude to Dr. Mohsin R. Anjum, Dr. Amjad Nisar, and Dr. Shafqat Hussain for their selfless assistance and direction.

In closing, I would want to thank everyone who has helped me during this research.

Abstract

The development of a highly active and low-cost catalysts for OER applications is very demanding. To improve the electrocatalytic performance of the catalyst, in this work, four Ni-Fe LDHs were synthesized by employing hydrothermal method with controlled stochiometric ratio of Ni and Fe. The synthesized LDHs catalysts were systematically investigated by XRD, SEM, EDX and FTIR. The electrocatalytic activity and chemical stability of catalysts were thoroughly explored by using electrochemical workstation. It is found that among other developed catalysts, Ni_3Fe_1 LDH electrocatalyst having high porosity, large specific surface area and high electrical conductivity exhibits highest current density of 890 $mAcm^{-2}$, least amount of overpotential of 264.3 mV, lower Tafel slope of 32 mV dec^{-1} and higher stability, as compared to other LDHs electrocatalysts. The enhanced performance of the catalyst is considered due to the rise of defects in the lattice. These defects give an abundance of active sites that play a significant role for the electrochemical reactions, thus, serving as OER electrocatalyst. It is concluded that the synthesized electrocatalysts exhibit electrocatalytic activity exceptionally at low overpotentials with outstanding long-term durability. The results suggest that defect generation play an important role for the development of high-performance electrocatalyst for water splitting applications.

Table of Contents

List of Figures

List of Tables

Chapter: 1

Introduction

1.1 Need for renewable energy sources

With the technological advancement in modern society and the ballooning world population, the demands for sustainable, maintainable and easily available energy are exponentially increased [1]. The rampant and unbridled uses of primary energy resources due to rapid industrialization have created global warming and climate changes around the world. Also, these resources have deteriorated the quality of air and triggered energy security issues [2]. Clean and sustainable energy production and storage to fulfill global energy demand from volumes number of natural resources is inevitable [3]. Among these resources, solar energy is not only infinite in quantity, inexhaustible and extensively available but also free of cost as well. In addition to solar energy conversion, researchers have been working on wind energy conversion along with other cheap resources. Yet, complete and sustainable conversion is still a dream to be fulfilled in the future. In a alternative ways to this burgeoning global energy demand are being investigated and studied. Harvesting solar radiation to the fullest is a core problem in getting benefits from this abundant energy resource. However, the recent development in the electrode materials has provided an alternative pathway for energy conversion, electrical energy storage, and advancement in batteries and super-capacitors. These novel pathways of photo electrochemical energy conversion, water splitting, and high-energy storage devices have gravitated to the attention of researchers around the globe. Score number of researchers have been doing their best to provide an alternative solution to the growing problems of energy demands and storage [4].

Energy is a vital factor in modern life, and conventional fossil fuels presently account for a major part of the world's energy supply. Figure 1.1 illustrates the world’s total energy supply by fuels in 2019, with 80.9% of net-emission fossil fuels including 26.8% of coal,

30.9% of oil, and 23.2% of natural gas, respectively. Forecasts predict the growth of these more than 25% by 2040. Fossil fuels, on the other hand, are non-renewable and result in a net release of carbon dioxide (CO_2) into the atmosphere, which has already changed the global climate visibly [5, 7, 8]. Due to the overuse of fossil fuels, escalating environmental problems, and an expanding worldwide population, there is a great need for sustainable energy alternatives [9].

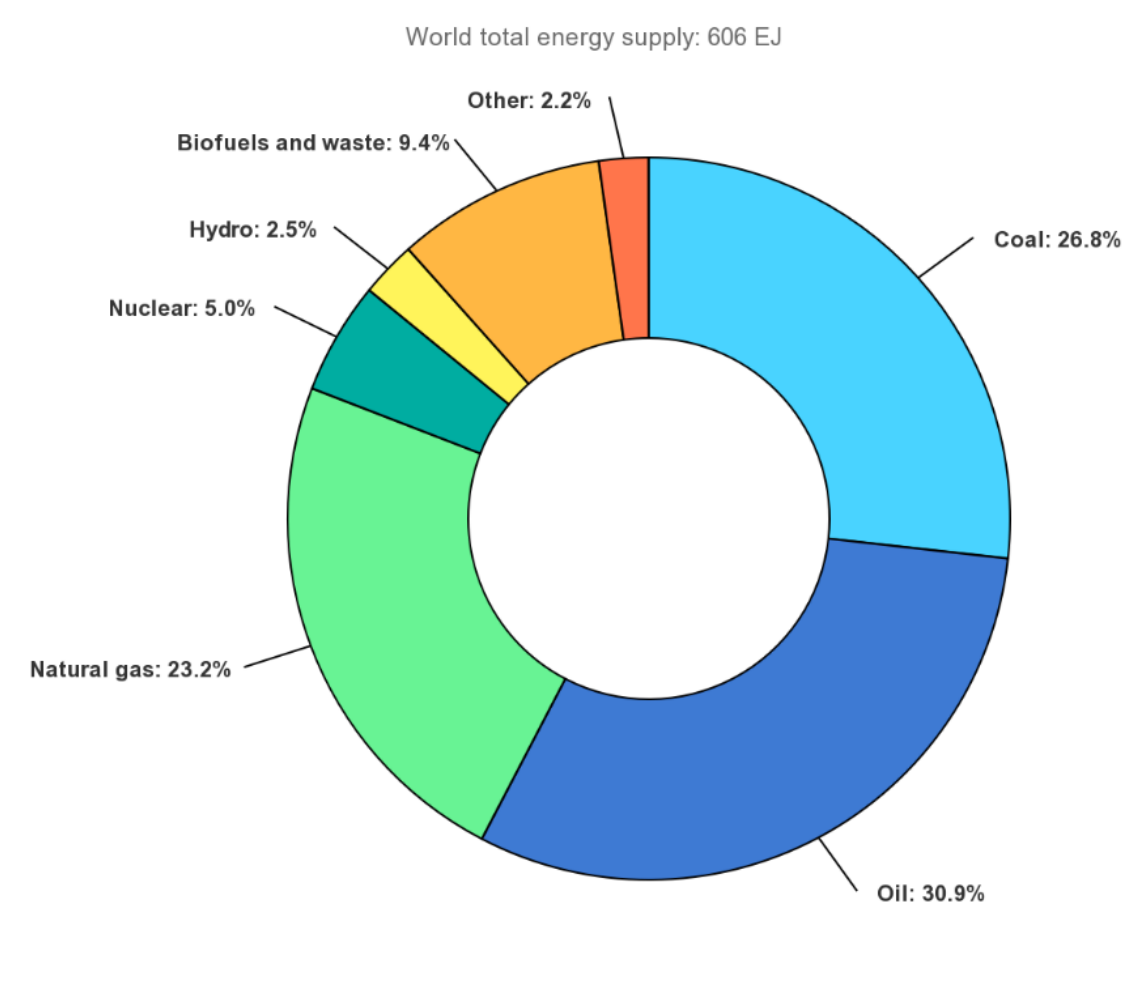

Figure 1- 1 World Total Primary Energy Supply 2019 [51]

Sunlight, wind and tidal energies are regarded as preeminent environmentally friendly renewable energy sources, and their ability to meet people's future energy needs has been well documented [10, 3]. One of the challenges confronting their largescale usage is their intermittent nature, and thus a need to equilibrate their output or store the energy for later

use [11]. Given the intermittent changes in the atmospheric conditions, the development of efficient storage technologies is important to enabling the growth of renewable electricity towards a situation where they can be the primary energy supply. One prospective approach is to develop electrochemical technologies enabling the efficient conversion of molecules in Earth's atmosphere (e.g., water, and carbon dioxide) into chemical fuels (e.g., H_2, hydrocarbons) via the integration of such systems with renewable electricity [9]. Figure 1.2 illustrates the available catalytic conversion pathways for renewable fuels. The universal feedstock can be efficiently transformed into useful products by electrochemical techniques coupled with renewable energies (e.g., solar, wind). Conversion of intermittent energies into chemical fuels with a zero net-emission would enable a sustainable supply of energy without any net change in the atmospheric conditions. This thesis is devoted to developing and understanding earth-abundant electrocatalysts with the required characteristics to split water into H_2 and O_2 as well as perform CO_2 reduction with high conversion efficiency.

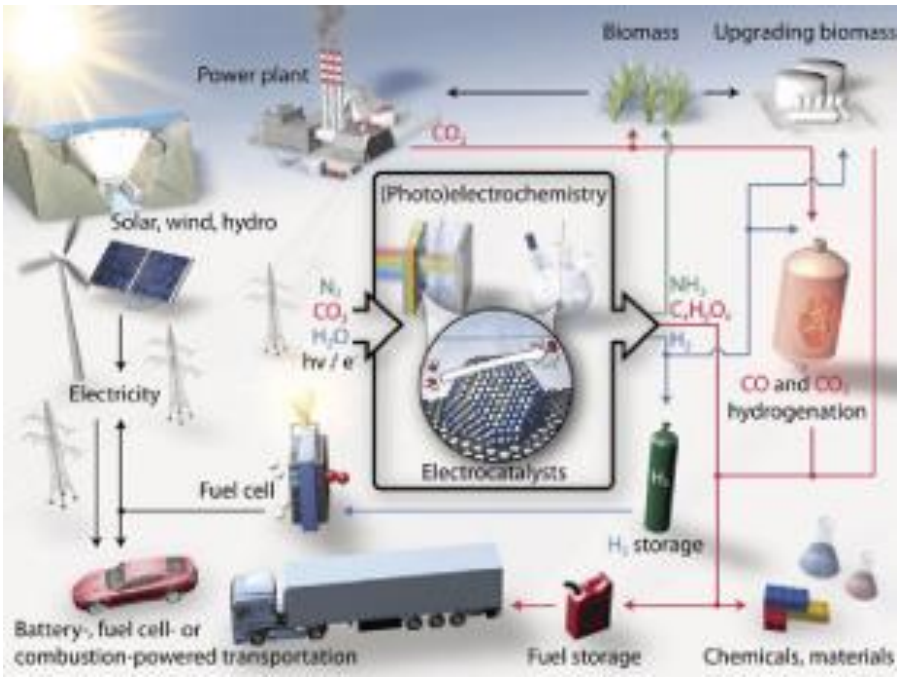

Figure 1- 2 Schematic of available energy conversions based on electrocatalysis [9]

1.1.1 Hydrogen Energy

Molecular hydrogen contains the highest energy density per mass ($0{:}0899 kg{=}Nm^3$) in any chemical compound and is also a carbon-neutral so chemical and would be an ideal energy carrier to power sustainable civilization. It is versatile to be used for heat, industry refining processes [12] and for providing electricity in stationary [13] and transport/vehicle applications via fuel cells [14] Presently, up to 96% of the hydrogen used in the world is derived from steam reforming of natural gas, and only about 4% of the hydrogen is produced from water decomposition [15]. Even though steam reforming is the cheapest way to produce hydrogen today, the large quantities of CO_2 emission prevent a large increase in this production technology [16]. Figure 1.3 depicts several solar energy-generated hydrogen processes, which include thermolysis, biomass, photolysis, and electrolysis. Thermolysis can split water straight at high temperatures, but it suffers from hydrogen and oxygen recombination at such temperatures, reducing its forward efficiency. Biomass conversion for hydrogen production is an inefficient and expensive idea, which cannot meet the global economy and energy demands without substantially decreasing the land necessary for the cultivation of food. Photolysis is not widely used because of its poor conversion efficiency and its instability [17]. The development of cost-effective catalysts and environmentally friendly technology is crucial for large-scale hydrogen generation in conjunction with renewables [18]. Hydrogen may be produced using a variety of methods, but water electrolysis using renewable power sources is the most straightforward and will likely play a significant role in the future [16]. Electrolysis of water has a distinct benefit, compared to other methods, of creating exceptionally pure hydrogen (> 99.9%), making it well suited to the unique requirements of industry, such as the fabrication of electronic components that need the addition of high-quality hydrogen [19].

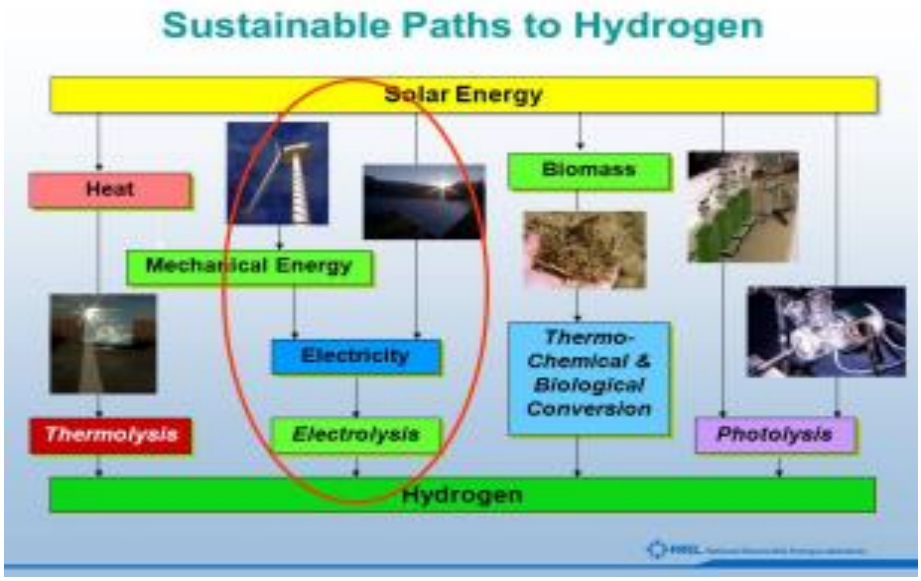

Figure 1- 3 Sustainable pathways for hydrogen generation from solar energy [16]

Renewable, CO_2-free energy sources that may be used with moderate efficiency include wind, solar, biomass, heat and hydro power. Together, they provide a long-term option for meeting our planet's energy needs, but a significant issue is the extremely varying spatial and temporal availability across the globe [20, 21]. To make the most of the potential offered by a given energy source, it is essential to have access to suitable energy storage facilities. Numerous processes, such as heating water or a solid mass, storing heat, compressing air, reducing carbon dioxide into reduced hydrocarbons, and making use of batteries, are all viable options for the storage and subsequent use of energy [22]. Hydrogen has garnered significant interest as a potential energy storage and transport medium within the Power-to-Gas (PtG) process chain as a result of its exceptionally high energy density as well as its capacity to recycle spent energy through the catalysis of environmentally friendly chemical reactions, meeting the demands of sustainable green energy [9, 23].

Although hydrogen has the potential to satisfy future energy needs as a sustainable energy carrier, the creation of hydrogen from sources other than fossil fuels accounts for just around 4% of the world's total output. Investing in a method of producing hydrogen that

does not rely on the combustion of fossil fuels will continue to be difficult so long as political incentives do not provide a financial incentive that favors the creation of green hydrogen [25, 26]. The electrochemical splitting of water, a technology that has been utilized in industrial production in the past and that is being used in industrial production today, is an easy and reliable means of creating sustainable hydrogen that does not emit CO_2 [24].

1.2 Uses of Hydrogen

The usage of hydrogen in the industry across the world is growing at a fast rate, with the bulk of it being used in the petroleum sector. This is because the hydrogenation process, also known as breaking hydrocarbons, is the preeminent method for producing fuels. Taking nitrogen and sulfur out of petroleum fuel requires a significant quantity of hydrogen to be added in its place. Hydrogen is in high demand since it is used in the creation of light molecules like methanol and in the saturation of petroleum-based hydrocarbons to make industrial reactants. Hydrogen has significant anti-corrosion applications and can scavenge free oxygen. Hydrogen is widely used in electrical generators as a cooling agent due to its efficient anti-corrosion properties. Due to the ease with which hydrogen (H_2) may be added to old molten plastic, regenerating polymer bulk material, the plastic recycling industry is booming. By decreasing their levels, both the petroleum and food sectors can raise the melting temperatures and oxidation resistance of oils and fats that are otherwise unsaturated. Fertilizer production utilizes a significant amount of hydrogen, accounting for approximately half of global usage [27]. The petroleum fuel cracking business consumes the remaining hydrogen. The conversion of metal oxides to metals necessitates a substantial amount of hydrogen. So far, hydrogen for use in stationary energy generation via fuel cells has not been a significant source of demand. However, because this method is being investigated for future usage, demand is expected to rise. Hydrogen has been put to use as a transportable fuel for many decades in the aviation sector, which involves the reaction between liquid hydrogen and liquid oxygen. It has been shown that this particular combustion results in the release of the greatest amount of energy at a stoichiometric ratio, all while being very inexpensive and simple to work with. As a result of the enormous volumes of hydrogen that are necessary

for rocket engines, this accounts for a significant fraction of the world's hydrogen consumption. The use of hydrogen as a car fuel is still in the early stages of development, but it is expected to grow over time as technology advances. [28].

Unfortunately, more than 90 percent of the energy was extracted from fossils. The process of splitting water into its component hydrogen and oxygen molecules is an efficient way to get hydrogen energy in a manner that is both clean and sustainable. The created hydrogen may subsequently be stored and oxidized (in an air or fuel cell), which results in the release of energy and the regeneration of water, creating a cycle of carbon-neutral fuel production and consumption. The reaction that occurs during water electrolysis may be broken down into two distinct phases: 1) The hydrogen evolution process, often known as the HER, and the oxygen evolution reaction (OER). As a result of the inherent slowness of the oxygen evolution reaction (OER) kinetics, the first half of the reaction is widely regarded as the essential bottleneck in the development of efficient electrolyzed water. This is because the OER kinetics require a significant amount of time to complete. As a result, developing an effective electrocatalyst for OER is extremely desirable.

1.3 Nature of Water Splitting

The molecular systems are constantly broken down, largely due to the oxidative destruction of biomolecules [29], but plants constantly rebuild the system by new synthesis of biomolecules at the same rate as they decompose. This principle distinguishes natural water splitting from the artificial method. The photosystem II (PSII) catalytic system uses its core group [$CaMn_4O_5$] to oxidize water. Five oxo-bridges link the metals in the core cluster in a configuration that is not the same as a normal cubane and has an additional manganese site [30]. As reactants, water molecules are transported around the inorganic core complex through a protein shuttle. One of the oxygen atoms is slightly weaker bonded, allowing it to obtain a small negative charge greater than the valence of -2 and thus play a role in the process of dioxygen formation [30].

For a long time, scientists have tried to make sense of oxides with oxygen coordinated in a cubic structure around a metal center, such Mn or Co atoms, without or containing redox inactive metals [31, 32]. Throughout the catalytic cycle, the valence electrons of the active

metal undergo a series of reversible electron transfer events to increase its oxidation state in oxo bridging to -OH_2, -OH, and -O - O species [33, 34]. Artificial bio-inspired systems use molecular structures that mimic these circumstances, which is useful since oxidative damage is a prevalent issue in biological systems but there is no continual anabolic pathway to rebuild and repair them. Large-scale artificial water splitting using bioinspired systems is impractical since these systems often fail before a commercial electrolyze.

1.3.1 Electrochemical Water Splitting

Advice for the design and manufacture of electrocatalysts requires a thorough understanding of the water splitting process. First, we'll take a brief look at the water-splitting process in general, and then we'll dive into the HER and OER processes in further detail in the next chapters. The Thermodynamics of reactions and electrode potentials are better understood as a result. Electrode kinetics data is provided, and an effective electrocatalyst is discussed in terms of reducing operating potentials. Last but not least, this chapter concludes with a discussion of the features used to evaluate electrocatalyst performance, thereby facilitating the selection of efficient catalytic materials.

1.3.2 Water Electrolysis Cell

In an electrolysis cell, such as the one seen in Figure 1.4, there was a cathode and an anode electrode which were placed in an aqueous electrolyte to produce hydrogen and oxygen. When a large enough potential difference is created between the electrodes, electrons will flow from the anode via the circuit to the cathode, resulting in an electrolytic reaction. The cathode is responsible for HER, which results in the formation of hydrogen gas whereas the anode is responsible for the oxidative OER. To speed up and more thoroughly complete the chemical transformation, either acidic or alkaline conditions may be used. These circumstances include high concentrations of ionic charge carriers viz., protons/hydronium ions or hydroxide ions.

The following reaction pathways can be used to describe the HER and OER in alkaline solution:

HER: $H_2O + 4e^- \rightarrow ½\ O_2 + 2H^+ + 2e^-$ (1.1)

OER: $4HO^- \rightarrow 2H_2O + 4e^-$ (1.2)

The reactions in acidic conditions are represented by:

HER: $4H^+ + 4e^- \rightarrow 2H_2$ (1.3)

OER: $2H_2 \rightarrow O_2 + 4H^+4e^-$ (1.4)

1.3.3 Electrolyte in Electrolysis of Water

In water electrolysis, water serves as both the reactant and the electrolyte. The electrolyte is often extremely acidic or alkaline, and many reaction processes are involved. The stability of the catalyst and cell material during extended periods of operation is impacted by such circumstances. The concentration has a significant impact on the resistance of the electrolyte, which is an essential aspect to optimization. Concentrated alkaline and acidic electrolytes have almost identical conductivities [6, 35]. A KOH-containing alkaline electrolyte has a conductivity of $2.7Scm^{-1}$ at 35 weight percent and $2.8Scm^{-1}$ at 45 weight percent at 200 [36]. Alkaline electrolyte corrosion has historically been found to be less severe and simpler to regulate than acidic electrolyte corrosion, leading to less expensive cell materials and upkeep. Furthermore, gas purity is increased by employing an alkaline electrolyte [37]. When KOH and NaOH were compared, the latter exhibited a somewhat lower ionic conductivity and produced greater corrosion. Because of this, when the same circumstances were applied, NaOH developed less hydrogen than KOH [38].

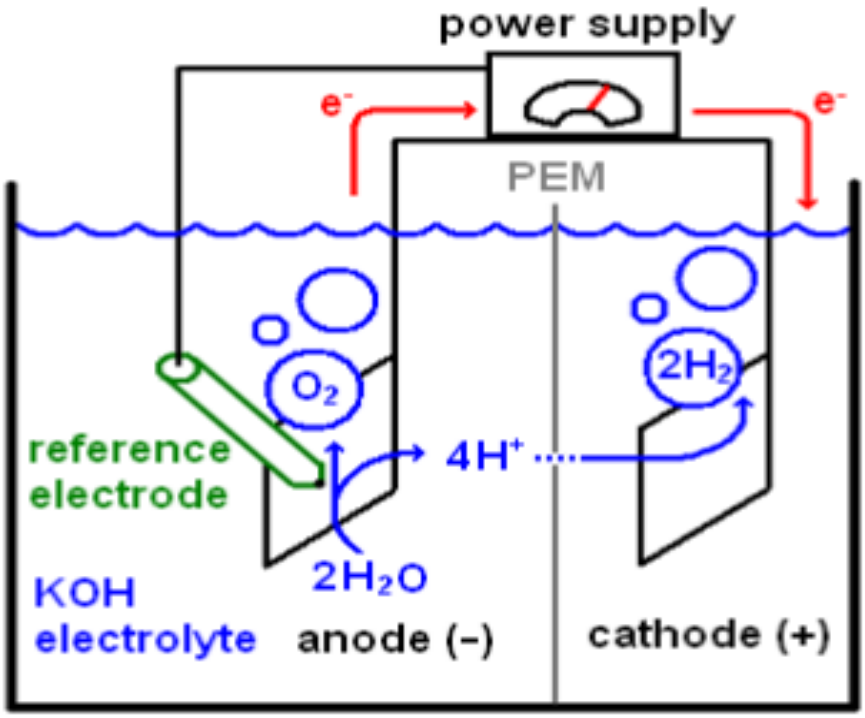

Figure 1- 4 A pictorial representation of a water electrolysis cell

1.3.4 Mechanisms of HER and OER

Understanding the HER and OER processes at the electrode/electrolyte interface may shed light on the catalyzed water splitting process. HER stands for hydrogen evolution reaction, while OER is for oxygen evolution reaction. This research explores the use of electrocatalysts in acidic and alkaline environments for the HER and OER, respectively. Therefore, the processes behind each reaction will be explained just for specific electrolyte circumstances to keep the discussion concise and clear. Both reactions follow a standard five-step method, any one of which may be the rate-determining step [39]

• Electrochemical reactions involving the transfer of reactive species (H_3O/H^+ or OH) from the electrolyte solution to the catalyst electrode surface.

• Surface adsorption

• Surface charge transfer reactions or chemical rearrangement

• Surface diffusion

• Desorption as H_2 or O_2 gas

1.3.5 Hydrogen Evolution Reaction (HER)

In general, HER follows one of two reaction mechanisms [40], and figure 1.5 depicts a pictorial representation of these pathways. However acidic medium possesses two mechanisms:

In the first phase, known as the proton discharge step, The Volmer process (wherein a proton is adsorption onto an electrode surface)

$$H_3o^+ + e^- \rightarrow H^* + H_2O \tag{1.5}$$

After that, either The Heyrovsky reaction, in which the adsorbed hydrogen atom bonds directly to a hydrated proton, or the Tafel reaction.

$$H^* + H_3o^+ + e^- \rightarrow H_2 + H_2O \tag{1.6}$$

$$H^* + H^* \rightarrow H_2 \qquad (\textit{Tafel Reaction}) \tag{1.7}$$

where two hydrogens that are adsorbed together diffuse and mix along the surface of the electrode. It might be the first (equation 1.5) or second (equations 1.6 or 1.7) reaction step in the mechanism, whichever one it is, it will be the step that determines the reaction's pace. According to Conway [40], the leading mechanism is determined by hydrogen deposited on the electrode's surface area. Tafel slope may be utilized to determine the prevailing mechanism in this scenario. A Tafel slope near 39 mV dec^{-1} or 29 mV dec^{-1} is required for optimal surface coverage of adsorbed hydrogen suggested by Heyrovky or Tafel reaction dominance.

The Volmer reaction predominates with low H_{ads} surface coverage, with a Tafel slope of 121 mV dec^{-1}. It's important to keep in mind, however, that the Tafel slope may be affected by various variables and can vary greatly even for the synthesis of the same substance

[41]. Only when there is a distinct R.D.S. do the aforementioned values occur, and even then, no step is usually noticeably slower than the rest. Therefore, the reason for a material's particular Tafel slope is not always obvious.

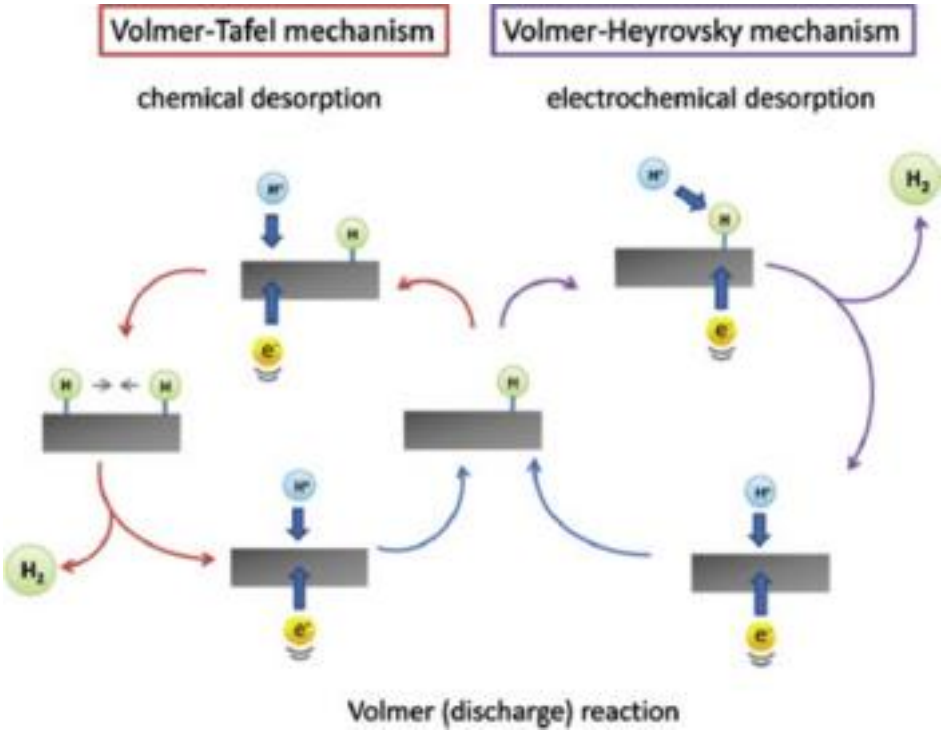

Figure 1- 5 The mechanisms of hydrogen evolution in acidic media [42]

1.3.6 Oxygen Evolution Reaction (OER)

The oxygen evolution reaction is more complicated than the HER because it includes the exchange of four electrons. Because the OER has a large number of possible reaction intermediates, the exact reaction mechanistic pathway is less well defined [43]. Many possible mechanistic schemes for the OER have been proposed over time [44] as shown in figure. 1.6. [43] The first step in every OER is the OH species onto the catalyst surface adsorption, and subsequent intermediate reaction steps often include many additional surface-adsorbed intermediates [43]. It might be challenging to pinpoint the rate-determining phases in the OER because to the lack of clarity in response pathways.

Mechanism I	Mechanism II
1. $2OH^- \rightarrow 2OH + 2e^-$	1. $2OH^- \rightarrow 2OH + 2e^-$
2. $2OH + 2OH^- \rightarrow 2O^- + 2H_2O$	2. $2OH + 2OH^- \rightarrow 2O^- + 2H_2O$
3. $2O^- \rightarrow 2O + 2e^-$	3. $2O^- + 2MO_x \rightarrow 2MO_{x+1} + 2e^-$
4. $2O \rightarrow O_2$	4. $2MO_{x+1} \rightarrow 2MO_x + O_2$
Mechanism III	**Mechanism IV**
1. $4OH^- + M \rightarrow 4M - OH + 4e^-$	1. $2OH^- \rightarrow 2OH + 2e^-$
2. $4M - OH \rightarrow 2MO + 2M + 2H_2O$	2. $2OH + 2OH^- \rightarrow 2H_2O_2^-$
3. $2MO \rightarrow 2M + O_2$	3. $2H_2O_2^- \rightarrow O_2^- + 2H_2O$
	4. $2O_2^- \rightarrow O_2 + 2e$

[a] *M denotes the electrode surface.

Figure 1- 6 Possible oxygen evolution reaction pathways in alkaline media [45]

IrO_2 and RuO_2, which both have a low overpotential and a Tafel slope, are the OER electrocatalysts that represent the current state of the art. These catalysts, however, are not suitable for mass scale and cannot be used for water split enterprises to develop cost-effective H2 energy resources [46]. This is since these catalysts are both scarce and expensive. The creation of low-cost catalysts that are capable of OER with high efficiency and activity has been the focus of major research efforts in recent years. These catalysts should be based on earth-abundant transition metals and should be able to be produced easily. This consists of compounds based on transition metals that are both inexpensive and have been researched for their potential use as OER catalyst replacements. From the point of view of their elemental make-up, Fe and Ni have garnered a lot of attention as potentially useful earth-abundant transition metals that may be used in the building of reliable OER catalysts [46].

According to the findings of a recent study conducted by Gao and Yan, the usage of mixed nickel and iron hydroxides in OER applications has been growing in popularity over the last several decades. Anions and water molecules in the interlayers create a charge balance for LDH's, These Nickel Iron LDH's have been demonstrated to exhibit small overpotentials and small Tafel slopes for OER under alkaline conditions, both of which are important catalytic signals [47].

Two-dimensional layered nanomaterials termed anionic clays are comparable in composition to the hydrotalcite $Mg_6Al_2(OH)_{16}CO_3.4H_2O$, which was discovered in 1842 and first synthesized in 1942. However, LDHs' ornate late-1960s architecture was complex. In these inorganic compounds, positively charged divalent metal cations, denoted by the symbol M^{2+}, are evenly dispersed throughout, and they coordinate octahedrally to hydroxyl groups to produce the compound denoted by the symbol $M(OH)_6$. In some instances, M^{2+} ions are partially replaced by M^{3+} ions [47]. They are constituted by a sheets structure with formula $M^{2+}{}_{1-x}\, M^{3+}{}_{x}\, (OH)_2](An^-)_{x/n}\, yH_2O$ where M^{2+} and M^{3+} denote divalent and trivalent respectively. A^{n-} is a charge compensating anion that is injected between the layers of brucite that make Ni-Fe layered double heterostructures (LDHs) are representative of a representative class of two-dimensional (2D) layered nanosheets. These nanosheets are constructed using a host layer that has the appearance of brucite and is built up of nickel oxide octahedra that are coordinated by hydroxyl groups. Additionally, these nanosheets contain a fraction of Fe^{2+}/Fe^{3+} that is substituting at Ni sites.

A deeper knowledge of OER reaction processes is needed to design effective OER catalysts that exhibit the features that enable fast kinetics. It is important to note that the electrodes on which the reaction actually place in today's industrial alkaline electrolyzes usually consist of nickel-based materials [49]. Al layer of hydroxides with a variety of topologies and degrees of hydration will develop as the cycling process continues. Some studies investigated how the OER might be affected by changing amounts of iron in nickel hydroxides, but they made no mention of the LDH structure in their findings [48]. Others have detailed results of Ni and Fe elements in hydroxides that were chemically bulk-synthesized, electrodeposited, or sputtered [50].

It is widely known that the atom arrangement and material structure have a significant impact on the electrochemical activity of any catalyst. It is generally acknowledged that a low degree of crystallinity can result in a large number of defects that are regarded as ideal active sites. While reviewing Ni $(OH)_2$ materials, Hall et al. found that it is still unknown what causes the improved efficiency, whether the electron vacancies are the product of contaminants or a very high degree of disorder. Owing to their rough surfaces,

considerable structural disorder, and greater charges transfer rate due to the low order range characteristic of the material, amorphous Ni-Fe hydroxides and sprayed Ni-Fe oxides are thought to be particularly good catalysts [61]

Chapter: 2

Literature Review

Layered double hydroxide, also known as LDH, has lately gained a lot of attention due to the distinctive two-dimensional structure it has as well as the several possible uses it may have. For instance, catalyst [52], anion exchangers [53], adsorbing materials [54], and so on. [Note: The LDH may be identified due to the presence of components that are similar to hydrotalcite. Hydrotalcite ($Mg_6Al_2(OH)_{16}CO_34H_2O$) is composed of Mg $(OH)_2$ layers in which Al^{3+} has replaced some of the Mg^{2+}, followed by layers of the anion (CO_3^{2-}) to neutralize the positive charge of the Mg $(OH)_2$ layers. This process is repeated until the structure of hydrotalcite is complete [55].

LDHs, as a class of ionic solids, is characterized by a layered structure with the general layer sequence [AcB Z AcB]n, where c is metal cation layers, A and B are hydroxide (OH-) anion layers, and Z is various anions and neutral molecules (such as water) [56]. Longer repeating periods may result from lateral offsets between the layers.

The positive layer (c) of the most studied class of LDHs is composed of divalent and trivalent cations and can be represented by the formula:

$[M_{1-x}^{2+}Mx^{3+}(OH)_2]^{x+}[A_{x/n}]^{n-}\ mH_2O$

where X^{n-} is the intercalating anion (or anions).

M^{2+} can be any of the following: Ca^{2+}, Mg^{2+}, Mn^{2+}, Fe^{2+}, Co^{2+}, Ni^{2+}, Cu^{2+} or Zn^{2+}, and Ni^{3+}, which is a trivalent cation that may be derived from the same atom as M. The range $0.2 \leq x \leq 0.33$ has been found to contain fixed-composition phases. In some cases, x can be greater than or equal to 0.5, indicating the presence of a phase transition [57].

We can easily gauge the structure of layered double hydroxides by analogizing the brucite structure, which has a general formula of $Mg(OH)_2$. Due to the close packing of the

hydroxide ions in brucite and the complete occupancy of the alternate octahedral sites by Mg^{2+} ions, neutral hydroxide layers are formed. Many of these hydroxide layers stack on top of one another due to Vander Waal's attraction force, resulting in a 0.48nm basal spacing. Anions intercalating between the layers of layered double hydroxide structure may be responsible for the formation of the mixed metal hydroxide layers with a positive charge in brucite, which is similar to the structure of a layered double hydroxide structure with a positive charge $[M_1x^{2+}M_x^{3+}(OH^-)_2]^{X+}$. Anions and metal hydroxide layers in the interlayer region can be linked together by hydrogen bonds in the interlayer water molecules, stabilizing the crystal structure of layered double hydroxide. Base spacing increases from 0.48 nm in brucite to 0.77 nm in hydrotalcite due to the intercalation between metal hydroxide layers of anions and water molecules.

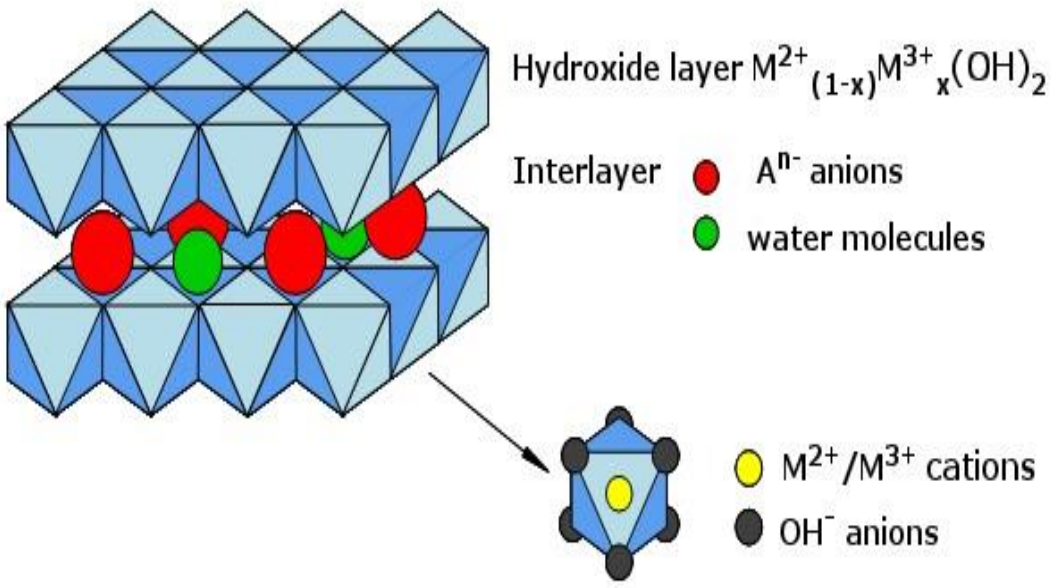

Figure 2- 1 Layered double hydroxide crystal structure [11]

Hydrogen (H_2) is widely considered to be one of the most promising zero-emission energy sources of the 21st century [58]. However, more than 90 percent of the energy that comes from hydrogen comes from fossil fuels [59]. One of the most fundamental and difficult to solve from a technical standpoint is the challenge of developing fossil fuel alternatives that do not pollute the environment. Obtaining hydrogen energy by water splitting is cheap

and sustainable from an economic and ecological standpoint [60]. Hydrogen is produced at the start of the carbon-neutral fuel production and consumption cycle, then stored and oxidised (by burning air or in a fuel cell) to release energy and replace water [61].

To overcome the energy barrier of the HER and OER, which occur at the cathode and anode, respectively, in a standard water electrolysis system, an external current is applied. The result is H_2 and O_2, respectively (237 kJ mol^{-1}). While the theory behind water electrolysis is straightforward, practical implementations on a wide scale to produce hydrogen gas are still in their infancy [62]. Water electrolysis was first demonstrated commercially in the 1890s. Electrochemical water splitting supplies barely 4% of world H_2 supply after more than a century of research [63], owing in large part to high costs and low efficiency. In actual use, the energy conversion efficiency of a typical commercial electrolyzed system range anywhere from 56% to 73% [64]. To solve this problem, we need to choose the right catalysts to increase the efficiency of the energy conversion. For the time being, catalysts based on noble metals continue to be the most effective catalysts for both HER and OER, with platinum being the most technologically sophisticated catalyst for HER [65, 66]. Because of this, finding earth-abundant catalysts that have a high activity level has become one of the top goals for the development of water electrolysis systems that are both cost-effective and efficient [67].

Generally, the water electrolysis process consists of two half-reactions: 1) water oxidation and 2) proton reduction. Electrocatalytic splitting of water is attractive because it can produce hydrogen gas and oxygen gas without the need for fossil fuels or the release of greenhouse gases. Typically, there are two stages involved in the electrolysis of water:

1) the oxidation of water

$$H_2O + 4e^- \rightarrow \frac{1}{2} O_2 + 2H^+ + 2e^- \quad (1.1)$$

2) proton reduction [14,15]

$$[2H^+ + 2e- \rightarrow H_2] \quad (1.2)$$

Electrochemical water splitting (WS) is a clean and efficient method for producing hydrogen that may be readily combined with other renewable energy sources including solar, wind, and wave power. Widespread acceptance rests on the two processes that make up WS: the oxygen evolution reaction (OER) and the hydrogen evolution reaction (HER). Both anodic OER and cathodic HER have significant excess potentials [68, 69] limiting the practical applications of WS. To reduce WS overpotentials, an efficient catalyst must be developed.

OER and HER are currently best catalyzed by Ru/Ir and Pt-based materials, respectively [70, 71]. Despite this, the high cost and scarcity of WS catalysts are a major barrier to its widespread use. Due to the inharmonious pH of the optimal electrolyte, it is also difficult to adequately activate WS when the catalysts are un an integrated electrolyze. This makes the process more challenging. In addition, catalyst stability is an important consideration when putting them to use. The need to develop a catalyst that can replace noble metal-based catalysts while also having high activity.

Catalysts based on Mn [72], Ni [65], Co [73], and Fe [74] have all lately received a lot of attention for WS research. Combining the two metals is predicted to improve electrochemical performance across the board, including in OER and HER. Furthermore, in OER and HER, the NiFe-based catalysts outperform all other electrocatalysts (such as those based on NiCo, NiMn, or CoFe). A universal electrochemical strategy was described by Duan's team in 2015 [84]. The technique's benefit of time and money savings makes it a feasible business route. This technique's NiFe-LDH on nickel foam has excellent OER (10 = 224 mV) performance and long-term high. The catalysts may be utilized in the actual world since the current density did not drop during the stability test.

Ni and Fe are often found together in the earth, thus it's interesting that even little concentrations of Fe in Ni (OH)2 electrodes may boost OER performance. The best OER catalyst, according to previous research, is $NiFeO_xH_y$. In addition, numerous studies have

shown that NiFe-based catalysts have excellent HER performance [75]. The abundance of Ni and Fe in Earth's crust means that commercialization costs can be reduced.

2.1 OER

Generally, the slowness of the oxygen evolution reaction (OER) is blamed for trying to halt progress in developing effective electrolyzed water's first half of the reaction [76]. As a result, it is imperative to develop a OER, which has recently gained worldwide attention.

It is also an important intermediate step in the production of MCF's and metal-air batteries. One of the key advantages of OER is its cheap cost and low environmental effect [77] batteries take oxygen from the air to obtain an extraordinarily high practical energy density while being light and affordable [78]. However, the sluggish kinetics of OER on the cathode might impair the performance of rechargeable metal-air cells. To increase the efficiency of energy conversion, it is crucial to develop new kinds of highly efficient and stable OER photo/electrocatalysts.

Overpotential and Tafel slopes of IrO_2 and RuO_2 show that these are the most advanced OER electrocatalysts. These catalysts, on the other hand, are usually in short supply and expensive, making them unsuitable for large-scale use in water-splitting industries and thus uneconomical H2 energy resources [79]. Researchers had the long-term objective of developing low-cost catalysts based on transition metals that are capable of OER with increased activity and efficiency. This covers low-cost catalysts based on transition metals that have been evaluated for their potential to act as OER catalysts. It is also important to point out that the OER overpotential of compositions including nickel and iron is also lower. For example, Ni hydroxide (Ni $(OH)_2$) electrodes may have a considerable influence on the performance of Ni-based alkaline batteries [80]. In addition to the groundbreaking work done by Wang and Sun, who compiled a summary of various transition metal-based electrocatalysts for the OER, hundreds of studies on electrocatalytic materials, notably for Ni/Fe-based systems, have been published in recent years.

Lu et al. synthesized NiFe-LDH on nickel foam hydrothermally. 200–300 nm thick mesoporous NiFe-LDH film shows good OER in 1.0 M KOH. Raman spectra showed that

the OER test converts NiFe-LDH to NiOOH, indicating that the NiOOH itself may be the real OER catalyst. It has been found by other research teams [81] that during the OER process, NiFe-LDH undergoes a structural transformation from hydroxide to oxyhydroxide, and that this oxyhydroxide phase may be the driving force behind the remarkable OER activity toward NiFe-LDH [82].

Perovskite tandem cells with NiFe-LDH on nickel foam electrodes were also used for water splitting by Luo and colleagues [83]. The solar-to-hydrogen conversion efficiency is up to 12.3 percent thanks to the excellent OER performance of NiFe-LDH on nickel foam. A new method of converting solar energy into hydrogen has been discovered using this combination.

A universal electrochemical strategy was described by Duan's team in 2015 [84]. The technique's benefit of time and money savings makes it a feasible business route. The NiFe-LDH on nickel foam that is produced by using this method has remarkable OER performance (10 = 224 mV) as well as strong current stability (50-250 mA cm-2) over an extended period (more than 50 h). The catalysts may be utilized in the actual world since the current density did not drop during the stability test.

To boost the efficiency of the catalyst, Long et al. successfully added Co into NiFe-LDH [85]. The authors synthesize ultrathin FeNiCo-LDH by switching the Fe salt for co salt at various points in the procedure. Atomic force microscopy (AFM) showed that as cobalt doping increased, LDH thickness reduced. Both FeNi9Co-LDH and FeNi8Co2 LDH have a thickness that ranges from 1.2-1.5 nm, with the former having a thickness of 1.5-1.8 nm. According to the findings from the LSV, the NiFe8Co2-LDH that is thinner and has a higher cobalt content has an onset potential that is 0.21 V lower. They reasoned that the increased OER performance must have been attributable to the Co replacement.

It was observed that heteroatom doping alters the chemical environment of metal sites on NiFeCr on carbon paper. Understanding this behavior requires heteroatom doping in NiFe-LDH. Furthermore, etching the replaced atoms and adding defects might boost NiFe-catalytic LDH's activity. Because Al^{3+} may partly dissolve in a high alkaline solution, Liu and colleagues [88] produced the faulty NiFeAlx- LDH. $Ni_3FeAl_{0.91}$-LDH

outperforms $Ni_3FeAl_{1.27}$, $Ni_3FeAl_{2.73}$, and nickel foam in terms of catalytic performance. At a potential of 1.60 V vs. RHE, $Ni_3FeAl_{0.91}$ has a current density of 235 $mAcm^{-2}$, which is much higher than Ni_3Fe (53 mA cm^{-2}), $Ni_3FeAl_{1.27}$ (120 mA cm^{-2}), $Ni_3FeAl_{2.73}$ (105 $mAcm^{-2}$), and pure Ni foam (20 $mAcm^{-2}$) [44].

2.2 HER

In recent times, there has been a lot of focus placed on HER as yet another significant side reaction in the Water Splitting process. Technology like the proton. exchange membrane [89, 90], CloNa electrolyzes [91], water-alkali electrolyzes [92, 93], and the solar splitting device [78, 93] all use it to great effect in the present clean energy revolution. However, its usefulness was limited by the need for a large amount of a non-noble metal catalyst in the electrolyte, which led to a high overpotential. An efficient and stable HER catalyst is difficult to come by. In addition, alkaline media provides the optimal reactive conditions for OER, HER must also exhibit great performance in an alkaline medium to get the best possible results when splitting water. Because of this, newly discovered electrocatalysts are more active in acidic and alkaline media. This is because the electric conductance of H_2SO_4 is higher than that of KOH.

As part of the water splitting process, the hydrogen evolution (HER) reaction converts + into - [94]. Even though the reactants are simple, and each hydrogen molecule only requires two electrons, the accumulation of energy barriers caused by the many elemental reactions leads to slow kinetics [95]. Different HER catalysts have been shown to have crucial roles in accelerating the reactions. Unlike other HER catalysts, platinum-based catalysts have essentially little overpotential at startup and quickly increase current with increasing voltage [96, 97]. However, because of their scarcity and high cost, they can only be used on a small scale, which encourages the development of low-cost alternatives with comparable activity and durability. Although several compounds based on nonprecious metals show considerable HER catalytic activity in acid [98], the absence of nonprecious equivalents for oxygen evolution catalysis has hampered the development of cost-effective water splitting devices in acidic solutions [99]. [98] Due to the abundance of highly active oxygen evolution catalysts that can function in alkaline conditions, innovative non-precious metal-based structures for HER catalysis in alkaline medium

have been developed. In this case, success may be attributed to the availability of oxygen evolution catalysts with very high activity levels [100].

Hydrogen evolution by electrocatalysis has been studied extensively during the last century. Whether a reaction uses the Volmer-Tafel or Volmer-Heyrovsky mechanism [101] depends on the catalytic surface. Both acidic and basic conditions are suitable for hydrogen evolution; however, the presence of various dominant species in the electrolyte generates different reactants and products in each elemental stage [95]. An alkaline environment triggers the Volmer process, which involves the dissociation of a water molecule adsorbed on a catalyst surface into a hydrogen atom and a hydroxide anion. Following adsorption, the H+ ion may either join with another H+ ion (produced in the Volmer step) to form a hydrogen molecule that escapes the surface (the Tafel step) or be attacked by another water molecule to make a hydrogen molecule and a hydroxide anion (the Heyrovsky step).

$H_2O + e \longrightarrow H_{ads} + OH^-$ (Volmer)

$H_{ads} + H_{ads} \longrightarrow H_2$ (Tafel)

$H_{ads} + H_2O + e \longrightarrow H_2 + OH^-$ (Heyrovsky)

Despite the common belief that metallic nickel is the most stable phase in alkaline solution under HER conditions [102], The generation of hydrogen using electrocatalysis has received a significant amount of attention from researchers over the last century. The catalytic surface determines whether a reaction employs the Volmer-Tafel or the Volmer-Heyrovsky mechanism [101]. Both acidic and basic circumstances are favorable for the evolution of hydrogen; however, the presence of diverse dominating species in the electrolyte creates different reactants and products in each elemental stage [95]. Hydrogen evolution may occur in either acidic or basic conditions. The Volmer process, in which a water molecule that is adsorbed on the surface of a catalyst is broken apart into a hydrogen atom and a hydroxide anion, is set in motion when an alkaline environment is present. This process includes the volatilization of water.

NiFeP [104], NiFeS [105], and NiFeN [106] exhibit outstanding HER performance, in contrast to NiFe-LDH and the other NiFe oxides, which show average catalytic activity toward HER in alkaline electrolytes. Nickel foam with permeable Ni-Fe phosphate was reported to be fabricated by Xing et al. [107], and this material shows off impressive HER performance. HER catalysts made of FeNiPx/NF (where NF stands for nickel foam) were created by Xiao and colleagues in 2017 [108]. The overpotential is very low value [109, 110]. Almost 400 hours of stability tests at 50 $mAcm^{-2}$ were conducted to validate the benefit of this in-situ deposited technique.

By performing in situ phosphatization of FeCo-LDH, the group led by Duan was able to synthesize FeCoP on nickel foam [111]. The FeCoP has remarkable HER performance as well as long-term stability in electrolytes with a range of pH values (pH = 0, 6.5, 13, and 14). The author developed a FeCoP model and calculated the adsorption behaviour of H_2O (-0.05 eV) to better comprehend the HER mechanism of FeCoP. The results reveal a more thermodynamically advantageous H_2O adsorption on FeCoP, which contributes to FeCoP's low reaction barrier in a basic electrolyte.

A separate study investigated similar results. Selenization of NiCo- LDH nanosheets resulted in the formation of $NiCoSe_2$ nanosheets on nickel foam [112]. To explain the remarkable performance of the HER in all pH electrolytes, the scientists estimated the adsorption energies of H_2O and H^+. According to the results of the calculations, $NiCoSe_2$ has a higher adsorption value than $NiSe_2$, which demonstrates that the presence of doped Co reduces the energy barriers for the adsorption of H_2O and H+ in $NiSe_2$.

Zhang et al. demonstrated that $(Fe_xNi_{1-x})_2P$ electrocatalysts are effective HER electrocatalysts [113]. The $(Fe_{0.048}Ni_{0.952})_2P$ was created by adjusting the amount of Fe doping in Ni_2P, and it demonstrates excellent HER performance and outstanding stability at high current density (100 mA cm^{-2}) throughout a wide pH range. Several models of $Fe_xNi_{84-x}P_{42}$ were developed to stand in for $(Fe_{1-x})_2P$ catalysts, and the free energy change associated with hydrogen adsorption (GH*) and water dissociation (GH_20) were determined. In addition, they calculated that the doped Fe might boost the activity of the active sites based on the charge density differential. The previous papers are crucial to the design and execution of neutral HER catalysts with high current density.

LDH is a lamellar ion crystal that consists of metal cations, interlayer anions, hydroxyl groups, and water molecules [114, 115]. Because of its novel lamellar structure and the mutual interaction between Ni and Fe, NiFe LDH has the potential to significantly boost OER performance [116, 117]. NiFe LDH has a low conductivity and no HER active sites, hence its HER performance in alkaline solution is poor, leading to a large overpotential and slow kinetics [118].

The HER activity of NiFe LDH has recently been studied in two main techniques. An approach that makes use of carbon nanomaterial composites to improve NiFe LDH's specific area and conductivity is intriguing. For example, Yao [119] created exfoliated NiFe LDH that was linked to defective graphene to create the heterostructure, and the resulting small overpotential for HER at 20 mA cm^{-2} was 115 mV. Adding noble metal dopants to NiFe LDH is yet another way to boost its efficiency [120]. To improve the electron structure and increase the number of active sites in NiFe LDH, Feng et al. [121] used a Ru-doping method. Indeed doping NiFe LDH with a noble metal may significantly alter its inherent catalytic activity, but the expensive cost and limited availability of noble metals prevent their widespread use.

Increasing the HER and overall performance of NiFe LDH in water splitting was proposed by Tang et al. as a technique of cation doping combined with H2 plasma reduction. One or more of the strong interface effects between metallic Ni and NiFe LDH, the synergistic effects of V-doping, O_v, and N_{iv}, and the improved electronic structures all contribute to the outstanding HER performance of the P-V-NiFe LDH NSA. At 10 mA cm^{-2}, its overpotential is 19 mV, putting it in direct competition with platinum-based electrocatalysts for HER activity. By decreasing the O* energy barrier, V-doping and Ov allow the P-V-NiFe LDH NSA to generate 100 mA cm^{-2} in OER at a voltage of just 295 mV. The P-V-NiFe LDH NSA is a great electrocatalyst for continuous water electrolysis due to its cell voltage of 1.43 V and its ability to drive 10 mA cm^{-2} for 1000 hours without degrading. This is because of the improved performance of HER and OER (122).

2.3 Synthesis Routes of LDHs Based Nanomaterials

Some of the most frequent techniques used in bulk synthesis include co-precipitation, ion exchange, heat absorption, and layer-by-layer deposition. Therefore, most popular method, called co-precipitation under low saturation settings, involves stirring a solution of the metals in the water while gradually adding a base (usually NaOH) at the appropriate molar ratio and concentration (Ref. [123]). Before being filtered, washed, and dried, the precipitate is allowed to mature in the mother solution. At each stage of the synthesis, the pH is controlled to maintain a constant range.

The ion-exchange method utilizes a previously synthesized LDH with a readily exchangeable interlayer anion [124, 125] as a starting point to create a unique LDH. There's a chance the exchange response isn't fully completed, making this approach inefficient. LDHs with tunable compositions may be prepared through co-precipitation or ion exchange employing a wide range of bivalent and trivalent cation combinations; however, these procedures frequently yield weakly crystalline materials, which can be improved with a thermal ageing step.

Calcination recovery, based on the so-called "memory effect" [126], is another well-known method for LDH formation. The interlayer anion is removed during calcination. This causes the layered structure of the layered double hydroxide (LDH) to collapse into a cubic phase and changes its name to layered double oxide (LDO). When the LDO is dissolved in water, the layered structure is rebuilt with a new anion intercalated between the layers, giving rise to a second LDH.

More recently, new techniques of synthesis have been developed with the goals of improving LDH crystallinity and obtaining LDHs with a morphology that is more consistent with and under control of the user. For instance, if urea is used as the hydrolysis agent, it is simple to create LDHs that have big platelets that are very thin and particle size distributions that are very narrow. Co-precipitation is the only method that, when a significant amount of time has passed, can provide these features. The technique was previously solely utilized to synthesize Al-based LDHs, but it has now been expanded to Mg/M/Al LDHs. These LDHs partially replace Mg with Fe or Al [127, 128].

The hydrothermal method is an additional method of preparation that enables the synthesis of LDH particles on a micrometer scale. This approach includes boiling a slurry of bivalent and trivalent metals (usually oxides or nitrate salts) to extract their LDH. Controlling heating temperatures and metal ratios modify LDH particle shape and size. This technique has been used to synthesize Mg/Al LDH [129]. Ni/Fe LDHs and CNTs/RGO composites for use in supercapacitors have recently been developed [130].

When using physical deposition methods, one of the most significant drawbacks was poor stickiness between LDH and conductor.; as a result, detachments can sometimes take place, particularly when the electrode is polarized. This is one of the primary disadvantages. It may be possible to increase film adhesion by reducing the number of particles but doing so will be difficult because this is a difficult problem. While conducting trials on co-precipitation and characterization, several different methodologies have been implemented to achieve this goal.

It is possible to lower the particle size to between 40 and 300 nm by carefully adjusting the co-precipitation conditions [131], and by separating the nucleation and ageing processes, it is possible to further tailor the sizes in a more precise range (60 to 80 nm) [132]. In still another method, a slurry of LDH is produced by aggressively churning a solution that contains both metal nitrates and sodium hydroxide and is carried out in a medium consisting of methanol. By subjecting it to further solvothermal processing, this LDH slurry can be converted into LDH nanostructures. [133].

Another method for the synthesis of LDHs is a procedure that is similar to that of sol-gel. Either alkoxide precursors are hydrolyzed and reacted with an alcohol, or alcohol is used as a solvent for the condensation reaction [134, 135]. This approach has several benefits that cannot be found in other synthetic processes a high specific surface area and narrow pore size distribution may be achieved with little effort, allowing for fine-grained control over the final product's structure and feel. Using the sol gel method, several other LDHs have been successfully synthesized, such as those having magnesium and aluminium [136], magnesium and gallium [137], magnesium and indium [137], nickel and aluminium [136], and zinc and aluminium [138].

The microemulsion approach is yet another potentially useful synthesis that can reduce the size of LDH particles to the nanoscale range. Typically, oil, water, and a surfactant make up the synthesis solution. Reverse microemulsions' water pools, which may be seen as nanosized reaction chambers, are exploited for this method. Because of this, this method is a powerful tool for managing the production of inorganic precipitates.

For the LDH to be useful for electrochemical applications. This is true regardless of the method that was used to synthesize the LDH. The surface of the working electrode, which can be made of metal or carbon, is typically coated with a film whose thickness is carefully managed to prepare LDH-modified electrodes [142]. A spin-coater deposits a measured amount of a chemically prepared LDH colloidal suspension., and then the coating is dried in air. This process is repeated until the coating is complete. This is referred to as spin-coating. Binders such as polytetrafluoroethylene, acetylene black, or Nafion are routinely used to promote mechanical adhesion. The method of (LbL) removal, which makes use of the electrostatic self-assembly process, can be utilized to accomplish the goal of obtaining LDH thin films. This method entails delaminating LDHs from individual nws, that are then alternated to species that have a negative charge and arranged on the electrode surface [143], which has been thoroughly researched by Sasaki and his colleagues [144].

One-step LDH synthesis on the conductive substrate may also be used to enhance the film's adhesion to the electrode substrate. The film's adhesion to the electrode substrate might likewise be improved using these ways. These processes are very quick, and they permit the synthesis of the LDH as well as the modification of the electrode at the same time. Additionally, they are not constrained by the form of the substrate in any way.

Electrochemical deposition is one of the most fascinating in-situ growth processes because it enables a conductive surface to be modified in one step without requiring further steps. The LDHs can be synthesized using a technique first reported by Kamath's group [145], which involves the electrocatalytic reduction of nitrates ions in a buffer comprising a bi-valent & tri-valent metal to produce a basic solution that allows the LDH to precipitate. Using those findings as a jumping-off point, the group led by Tonelli conducted an exhaustive analysis with the objective of identify the optimal experimental conditions for the modification of multiple electrode materials [146].

Ni-Fe LDHs are typically layered materials, therefore changing the Ni/Fe ratio, interlayer ionic composition, and/or porosity may result in a wide variety of changes to the materials' characteristics [149, 150]. This allows for a wide variety of possible applications. Because of this, Ni-Fe LDHs are now part of a class of materials that have a strong capability for the conversion and storage of energy [151].

Ni and Fe reserves on Earth are sizable, which might help keep production costs down. In the present day, two main methods are used to synthesize catalyst electrodes for water splitting [152]. The most common technique involves dripping a slurry of catalyst and conductive binder onto the electrodes [153-155]. But there are two problems with this approach: (i) The electrocatalytic performance is reduced because the slurry's electrically insulating binder reduces the contact area between the catalyst and electrolytes [156], and (ii) the attached catalysts are prone to detach from the electrode as a result of the rapid Hydrogen/Oxygen bubble production, leading to low stability. In order to get over these problems, people paired water splitting catalysts with conductive substrates such as nickel foam [157-159], FTO [160-163], iron substrates [164], stainless steel [165-166], nickel foils [167-169], copper foils [170-173], and carbon paper [174-176].

Although significant attention has been paid to Nickel foam as a conductive substrate, very few works use Nickel foil as a conductive substrate. There is still space for further research, especially in the case of Ni-Fe LDH synthesized by hydrothermal process using nickel foil as a substrate. No evidence was found in which Ni-Fe LDH was directly grown on Nickel foil by hydrothermal method and study the importance of the molar ratio of the salts on structural, morphological, and electrochemical properties.

In this research, a hydrothermal synthesis of Ni-Fe LDH on nickel-foil is proposed. Simply by adjusting the concentrations of Ni $(NO_3)_2 \cdot 6H_2O$ and Fe $(NO_3)_3 \cdot 9H_2O$, the Ni-Fe LDH was developed directly on Ni-Foil. Since Ni-Fe LDH was grown directly on Nickel foam, it exhibits great electrical conductivity between the nickel foil and Ni-Fe LDH catalyst layer and a strong physical bond. Because this synthesis method is straightforward, it can be implemented in industrial alkaline water electrolysis.

2.4 Research Objective:

- Synthesis of Ni-Fe LDHs by hydrothermal process. Various samples with a precise Ni/Fe stoichiometric ratio will be prepared.
- Structural and morphological analysis of the developed catalysts by using the XRD, SEM, EDX and FTIR.
- Study the importance of molar ratio of the salts on electrochemical Activity.

Chapter: 3

Materials and Methodology

3.1 Synthesis Routes

The synthesis of layered double hydroxides, also known as LDHs, makes use of many different approaches and pathways. In this study, we used a hydrothermal method that was both simple and economical. The following is a more in-depth description of the experiment.

3.1.1 Hydrothermal Method

Hydrothermal reaction was used in this study. Hydrothermal reactions are carried out by dissolving metal salts in solvents and then heating the resulting solutions to the appropriate temperature. The morphology and structure of LDH produced via the hydrothermal process can be controlled by adjusting reaction factors such temperature, pressure, reaction time, and molar ratio. All the intermediate and final phases of the synthesis pathways are depicted in the figure 3.1.

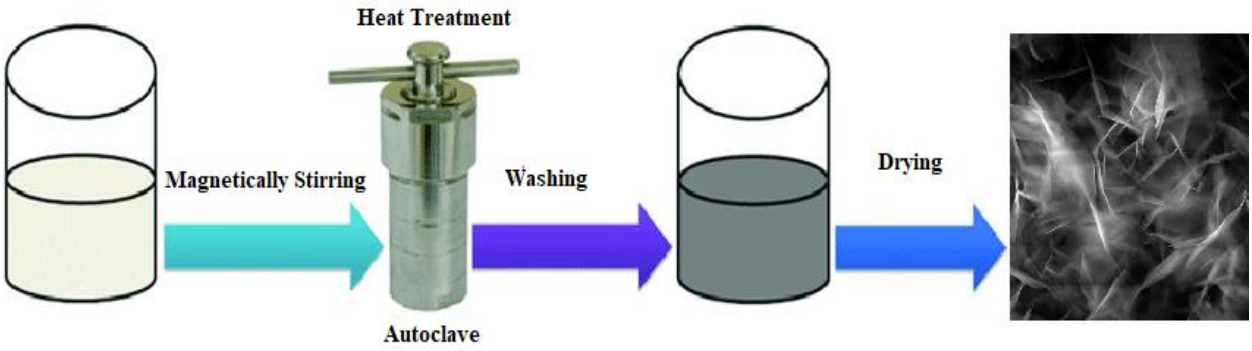

Fig. 3.1 Hydrothermal Synthesis Method for Ni-Fe LDH

3.1.2 Chemicals Reagents

Nickel-Nitrate Hexa-hydrate [Ni $(NO_3)_2 \cdot 6H_2O$], Iron Nitrate Nona-hydrate [Fe $(NO_3)_3 \cdot 9H_2O$], Urea CO $(NH_2)_2$, ethanol, sodium hydroxide and potassium hydroxide were purchased for the synthesis of Ni-Fe LDH. Deionized water was used to prepare all aqueous solutions. Besides, all the reagents were of analytical grade and were used

without further purification. All materials were purchased from Sigma Aldrich USA. For washing and cleaning the apparatus distilled water, acetone and commercial ethanol were used.

3.1.3 Treatment of Nickel Foil

To remove the surface NiO layers, Nickel foil was thoroughly cleaned with a dilute HCl solution by ultrasonication for 5 minutes, and then sonicated in Acetone, deionized water, and lastly in absolute ethanol for 3 minutes each.

3.1.4 Apparatus

The following items were utilized: beakers, magnetic stirrers, falcon tubes, funnels, pipettes, graduated cylinders, watch glasses, wash bottles, and Petri dishes. First, all of the apparatus was cleansed with distilled water, then washed with ethanol, distilled, deionized water, and finally washed with commercial acetone.

3.1.5 Instruments and Equipments

During the synthesis of Ni-Fe LDH, the following instruments and pieces of equipment were utilized: a digital balance; an ultrasonicator; a centrifuge; a Teflon-lined autoclave; a hot plate; and a hot air oven. A heating oven was used for reactions and drying purposes whereas centrifuge machine was for washing the materials.

3.2 Synthesis of Ni-Fe LDH

Ni-Fe LDHs were synthesized by a hydrothermal method, namely, Nickel-Nitrate Hexa-hydrate $Ni(NO_3)_2 \bullet 6H_2O$, Iron-Nitrate Nona-hydrate $Fe(NO_3)_3 \bullet 9H_2O$ with four different ratios and Urea $CO(NH_2)_2$ were dissolved in 35 mL of distilled water and stirred to form a clear solution. Ni-Fe Samples were successfully prepared with four different ratios of Ni $(NO_3)_2 \bullet 6H_2O$ and Fe $(NO_3)_3 \bullet 9H_2O$ keeping Urea fixed. These proportions are mentioned below

Table 3- 1 Ni-Fe sample proportions used in current study

Sr. No	**Sample Name**	**Ni $(NO_3)_2$•6 H_2O**	**Fe $(NO_3)_3$•9H_2 O**	**Urea**	**Ni $(NO_3)_2$•6H_2 O**	**Fe $(NO_3)_3$•9 H_2O**	**Urea**
		(mmol)			**(mg)**		
1	Ni_3Fe_1	21.42	7.14	142.857	218.1	100.1	300.3
2	Ni_2Fe_1	19.04	9.52	142.857	194	133	300.3
3	Ni_1Fe_1	14.28	14.28	142.857	145.3	200.1	300.3
4	Ni_1Fe_2	9.52	19.04	142.857	968.9	266.8	300.3

After stirring for an hour, the aforementioned solutions and nickel foils were transferred to four well-washed and cleaned autoclaves and closed very well. Then these auto-clave were kept in a heating oven sealed, and kept at 120° C for 12 hours. After performing this activity, the autoclave was cooled down to the room temperature naturally. The Ni-Fe LDHs were then cleaned three times with deionized water & ethanol before being dried at 80 ℃ for six hours.

Table 3- 2 Variation in key parameters enroute to the fine-tuned results

Sr. No	Sample Name	Changing Parameters	Fixed Parameters			
		Molar Ratio of Ni/Fe Salts (mmol)	Heat Treatment		Drying	
			Time (hrs.)	Temperature (°C)	Time (hrs.)	Temperature (°C)
1	Ni_3Fe_1	3:1	12	120	6	80
2	Ni_2Fe_1	2:1	12	120	6	80
3	Ni_1Fe_1	1:1	12	120	6	80
4	Ni_1Fe_2	1:2	12	120	6	80

For washing purposes, the solution was then transferred into a falcon tube and kept in a centrifuge tube. The machine was set at 8000 rpm for 10 minutes. The solution was washed again and again with Deionized water and ethanol until all the impurities were removed and the pH gets neutralized. After getting rid of all the impurities, the material was shifted into a petri dish and kept in a drying oven dried at 80 °C for six hours. All four reactions followed the same general procedure except for the different amounts of surfactant.

Figure 3- 1 Autoclave and liner used for reactions in a heating oven

3.3 Introduction to Characterizations Technique

For a given application, the material's properties must be accurately assessed and documented. No useful applications or activities may be performed on a material that lacks proper and prior understanding of the substance's physical and chemical properties. Several characterizations have been carried out to learn about the material's aforementioned parameters. The following sections of this chapter go into great detail about each of those points.

3.3.1 X-ray Diffraction Technique

XRD is the most important characterization technique for determining a material's crystal structure and crystallinity. Determining the orientation of an atom or grain in a crystal lattice or structure and the spacing between different planes from which material is comprised. In addition, the crystalline structure's size and internal stress can be measured using this technique.

3.3.1.1 Objectives of XRD

1. It identifies the crystallinity of a material.
2. It is utilized to differentiate between crystalline and amorphous forms.
3. To compute the material's lattice spacing.
4. Determine the average particle size

3.3.1.2 Working Principle

Constructive interference between monochromatic X-rays is the basis for the XRD's operation. A cathode ray tube generates monochromatic radiation by filtering out non-monochromatic X-rays. The rays are collimated so that they can be focused on the specimen. Bragg's Law is satisfied when these rays interact with the specimen, resulting in constructive interference. As stated in Bragg's Law, the diffraction angle and lattice spacing of a specimen are directly related to its wavelength of electromagnetic radiation. One way to express it is

$$n\lambda = 2d\ sin\theta$$

Where n denotes the order in which reflections are performed, X-ray wavelength is represented by λ, and a specimen's characteristic crystal plane spacing is represented by d. θ is the angle created between the incident beam and the lattice plane normal.

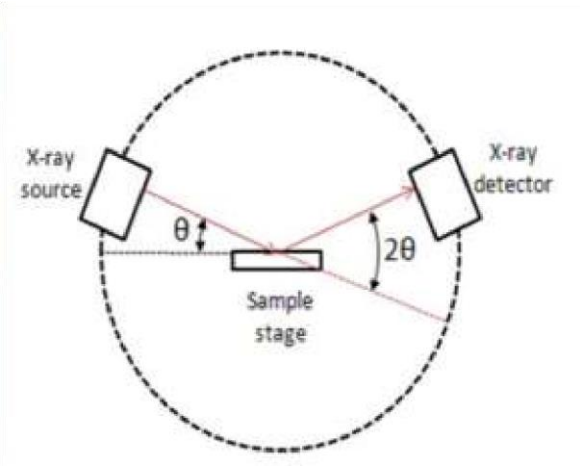

Figure 3- 2 Schematic diagram of XRD

3.3.2 Scanning Electron Microscopy

Electron scanning microscopes (SEM) use a focused beam of high-energy electrons to generate different types of signals at the surface of specimens. Signals from secondary electrons (SE) and backscattered electrons (BSE) are investigated and claimed. SEM reveals numerous sample characteristics, including chemical composition, surface morphology, and crystalline structure, among others. On predefined regions of the sample surface, the beam is scanned, and data are collected. The schematic of SEM is shown in the figure 3.3 below.

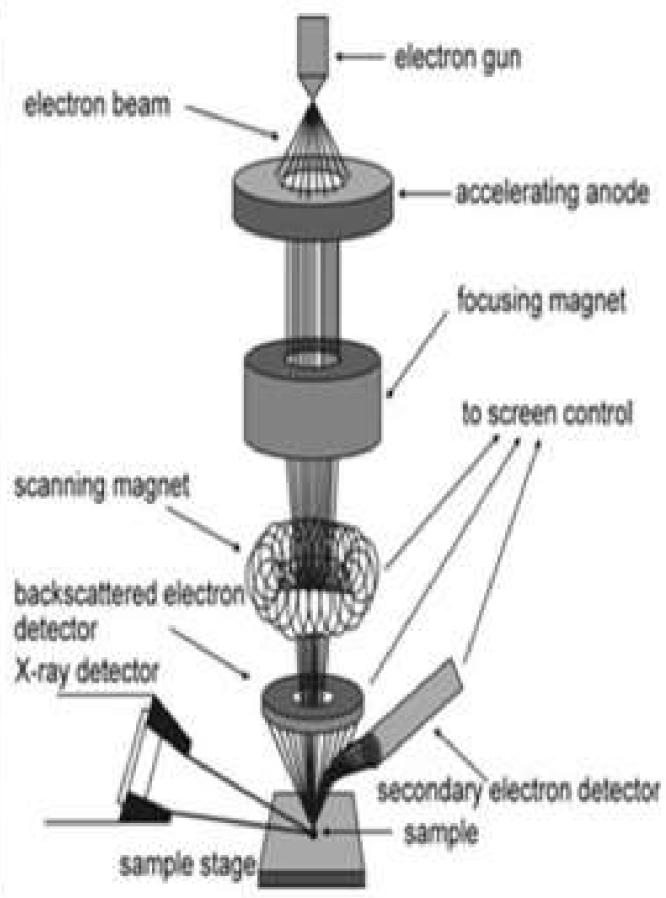

Figure 3- 3 Schematic diagram of scanning electron microscope

3.3.2.1 Objective of SEM

The surface of a material can be observed in incredible detail with SEM, which is an excellent method for examining the material's surface. It contains details on a variety of topics.

1. Texture (External Morphology)
2. Chemical composition
3. Orientation
4. Crystalline Structure

3.3.2.2 Working Principle

Electron beams are used to generate the image of a material, and electromagnetic fields are used to magnify it.

3.3.3 Fourier Transform Infrared Spectroscopy (FTIR)

3.3.3.1 Objectives of FTIR

1. Recognize organic, polymeric, and occasionally inorganic substances.
2. The characterization of unknown substances.
3. Identification of contaminant sources (in or on the materials).
4. Locate uncured or decomposing chemicals in failure analysis

3.3.3.2 Working Principle

The FTIR relies on molecules' ability to absorb light in the infrared region of the electromagnetic spectrum. Molecules that absorb light have a specific relationship to the bonds that make up their structure. It can be classified into the near, mid and far infrared areas, which are all within the range of 12800 to 10 cm^{-1} [177].

The process of the infrared absorption spectrum is based on molecular vibrations. When the specimen is subjected to radiation, its molecules absorb certain wavelengths of radiation. This alters the dipole movement of the sample molecules. As a result, the energy level of the specimen molecule is transferred from the ground state to the excited state. The frequency of the absorption peak is determined by the

energy gap. The dipole moments and energy level shifts are responsible for the change in intensity.

Table 3- 3 Frequency Range of different IR Regions

Infrared region	Range of frequency (cm^{-1})
Near IR	12800-4000
Mid IR	4000-200
Far IR	1000-50

The source produces the radiations. After passing through the interferometer, these radiations reach the specimen and are detected by the detector. Signals are amplified by an amplifier before being transformed into digital signals by an analog-to-digital converter. Finally, the signal is sent to a computer for Fourier transformation.

3.4 Electrochemical characterization

The electrochemical measurements were performed at room temperature using an electrochemical workstation (CHI660e, China) with a three-electrode configuration. In an electrochemical cell three electrode system was used. One is a working electrode which was Ni-foil on which Ni-Fe LDH was directly grown during hydrothermal. The second one is the reference electrode which is Silver Silver Chloride (Ag/AgCl) and the third one is a counter electrode of platinum wire. All potentials are reported against reversible hydrogen electrode (RHE), and a resistance correction was applied to all initial data for reflecting the inherent activity of the electro catalysts. A freshly prepared 1M KOH aqueous solution was used as the electrolyte.

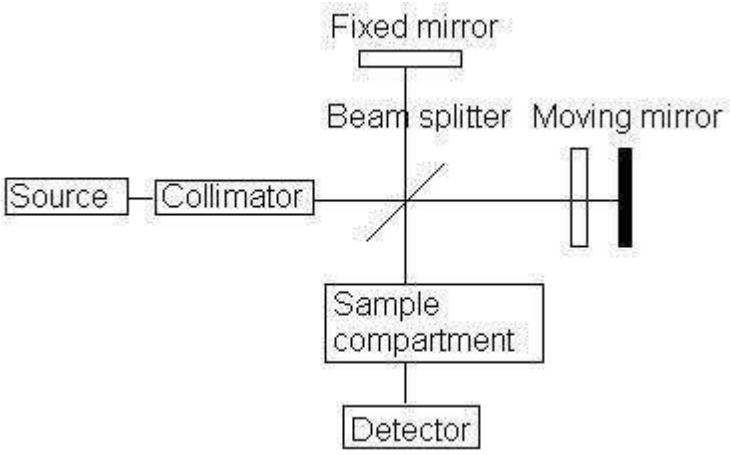

Figure 3- 4 Schematic of components of FTIR [178]

3.4.1 Linear Sweep Voltammetry

It is possible to perform linear sweep voltammetry with a defined potential range like that of potential step measurement. From the lower to the upper limit, a voltage scan is performed in the manner described below.

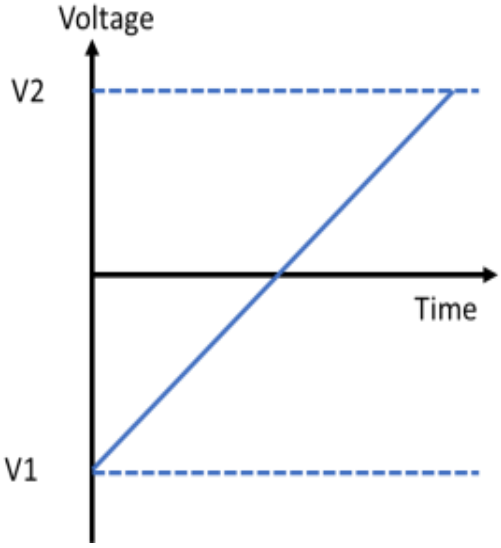

Figure 3- 5 Schematic representation of LSV

The slope of a line can be used to compute the scan rate. It all relies on the amount of time it takes to sweep the voltage range. Many factors influence the LSV curve's characteristics.

1. The rate at which an electron must be transferred

2. The chemical reactivity of electroactive species
3. The scan rate for voltage.
4. The response of current is plotted against the voltage

3.4.2 Cyclic voltammetry (CV)

Cyclic voltammetry testing shares several characteristics with LSV. In this procedure, the voltage is varied between two values at a constant rate, and when it reaches the value V_2, reverse scanning is conducted, and the voltage is returned to the value V_1. Figure 3.6 depicts a cyclic voltammogram for a single reversible electrode. The response when the voltage increases from V_1 to V_2 is identical to LSV. Reversing the scan alters the equilibrium position of the curve, resulting in oxidation. In this instance, the current flows from the electrolyte towards the electrode. When electrochemical reactions are done in a reversible manner, the CV exhibits particular features.

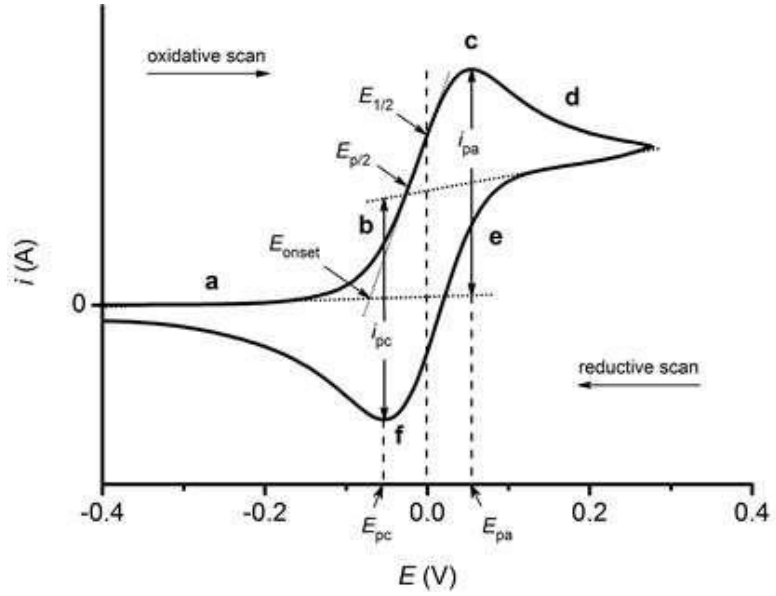

Figure 3- 6 Cyclic voltammetry curve illustration D. Lidzey, "Cyclic Voltammetry: Basic Principles & Set Up."

1. Current peaks are separated by a voltage of ΔE= $E_P^a - E_P^c$
2. The position of the peak voltage does not vary when the scan rate changes.
3. The ratio of the peak current yields the value $\frac{i_P^a}{E_P^c} = 1$
4. Peak currents are proportional to the square root of the scan rate.

3.4.3 Electrochemical Impedance Spectroscopy (EIS)

Electrochemical impedance spectroscopy (EIS) is a quick, non-destructive, and easily automated method for determining the electric characteristics of a wide range of materials. It involves applying a sinusoidal voltage and measuring the response of the current.

Nyquist or Bode plots are used to represent EIS values. An imaginary impedance value on the x-axis and a real impedance value on the y-axis are plotted in the Nyquist plot. The Bode plot displays data for low and high frequencies. Rp equals the difference between low frequency and high frequency resistance. The data at low and high-frequency can be seen on the Bode plot. There is an Rp value for the difference between low-frequency and high-frequency resistance. Warburg's element is connected in parallel to Rs and Rp to demonstrate the diffusion mechanism using an equivalent circuit [153].

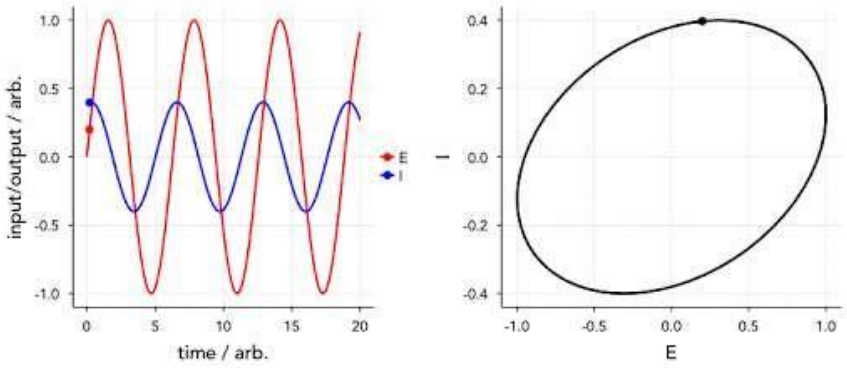

Figure 3- 7 Principle of Electrochemical impedance spectroscopy

3.4.4 Tafel slope

Tafel slopes are used to study electrocatalysts and reactants' Tafel behaviour. With an efficient electrocatalyst, the Tafel equation can be translated into logarithmic functions, which indicates a reduced overpotential and faster increase in current density. In addition to providing insight into the OER process, the Tafel slope indicates the rate-determining step. Exchange current density (j_0) is a direct reflection of the inherent rate of electron transport between electrode and analyte. Nevertheless, the complex OER process and large inaccuracies associated with exchange current density estimate j_0 are seldom employed in OER and HER.

$$\eta = b \times \log j + a$$

where, η is overpotential, j is the current density, and b is the Tafel slope.

3.4.5 Onset overpotential and overpotential

The applied potential at which the first signs of an apparent current arise is known as the "onset overpotential." It is unable to provide precise estimates due to the influence of intrinsic elements such as materials and the environment. Overpotential at 10 mA cm^{-2} is often used as a standard by scientists for quantitatively evaluating catalyst performance [178]. Overpotential at higher current densities is another criterion for evaluating nickel foam-based catalysts. So, ideally, a catalytic material would allow for a higher current density at a lower overpotential. The Ag/AgCl electrode and the saturated calomel electrode are used for standardization purposes (SCE) [179].

According to the formula presented below, the final data was analyzed and converted to the potential versus the RHE:

$$ERHE = EAg/AgCl + E^0_{Ag/Agcl} + 0.059 * pH \qquad (E^0_{Ag/Agcl} = 0.197V)$$

$$ERHE = ESCE + E^0_{SCE} + 0.059 * pH \qquad (E^0_{Ag/Agcl} = 0.242V)$$

3.4.6 Electrochemical active surface area (ECSA)

Catalysts' ECSA is measured by their electrochemical double-layer capacitance (C_{dl}), which provides insight into their reaction process. The C_{dl} may be calculated from CV curves by conducting experiments in a narrow potential range. In this way, researchers may easily get a series of five to ten CV curves at a range of sweep speeds, from five millivolts per second to two hundred. The ideal form for the generated CV curves is something close to a rectangle. By determining the difference in current density under the current potential ($j = j_1 - j_2$) and then linearly fitting this data with varying sweep speeds along the X-axis and j along the Y-axis, we can get the slope. The gradient is twice as steep as C_{dl}. Greater values suggest more exposed reactive sites at the surface and higher current densities [180].

3.4.7 Stability test

The stability of electrocatalysts is a crucial activity parameter associated with OER catalysis that can be measured in many methods. The cyclic stability is determined by the variation in linear sweep voltammetry (LSV) after 1000 cycle Voltametric scans. It can also be represented by a durability test, which measures the change in performance as a function of time at a certain current density (chrono-amperometry) or a specific applied potential (chronopotentiometry). Long-term Galvanostatic or potentiostatic operation is employed for its operation. The material is considered stable if its activity does not change following long-term polarization.

Chapter: 4

Results and Discussion

4.1 Characterization

4.1.1 Structural Analysis

The XRD was used to study the crystal structure and phase purity of the prepared samples. The XRD patterns of Ni_3Fe_1, Ni_2Fe_1, Ni_1Fe_1 and Ni_1Fe_2 samples are shown in Figure 4.1 &4.2. All patterns exhibit the characteristic reflections at 11.4°,22.95° and 34.3° corresponding to (003), (006), and (009) planes of the LDHs structures.

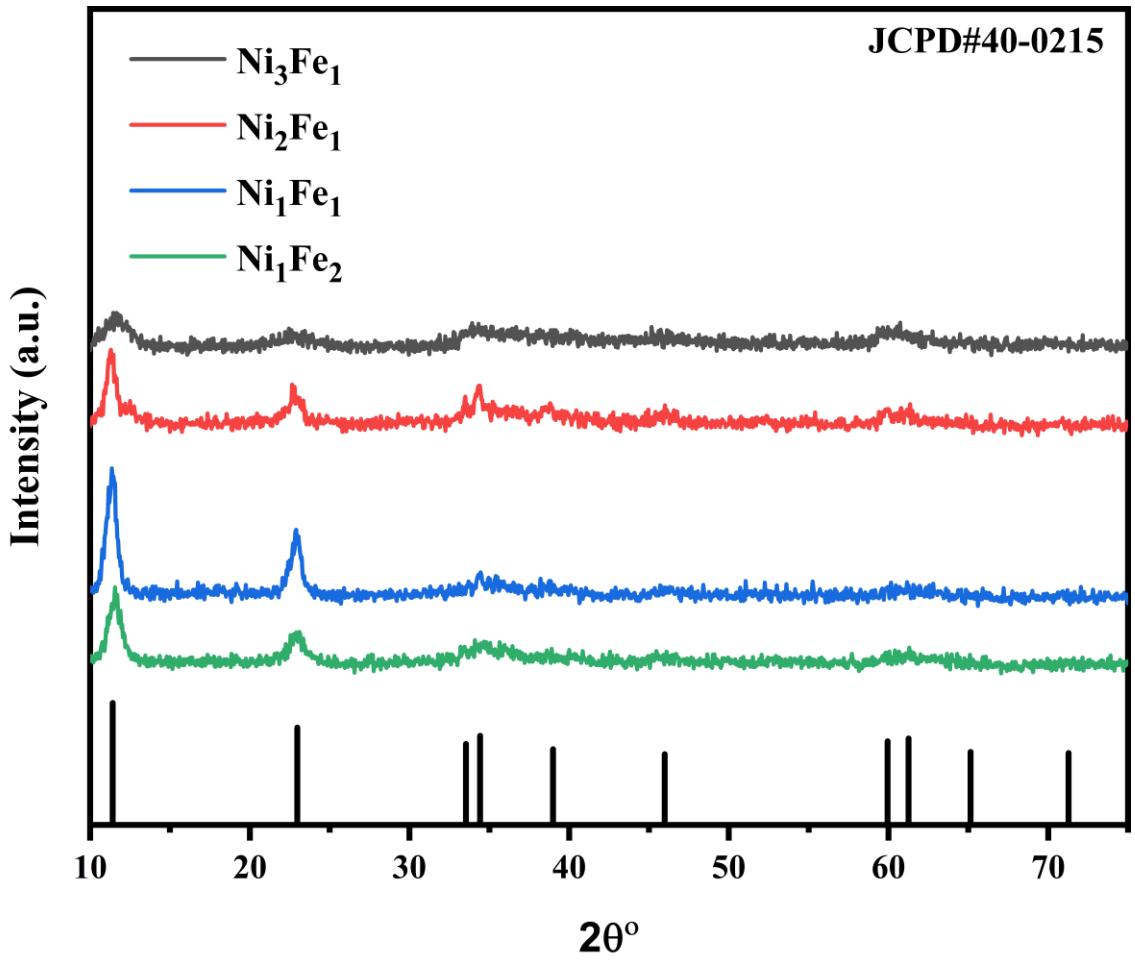

Figure 4- 1 XRD patterns of the synthesized Ni_3Fe_1, Ni_2Fe_1, Ni_1Fe_1 and Ni_1Fe_2

The pattern is consistent with the peaks that correspond to the rhombohedral structure of α–Nickel Iron LDH, which can be represented by the calculated pattern designated as JCPDS 40–0215. The peaks at 11.4°,22.95° and 34.3° are characteristics of compounds that are typical of the layered structure of the 3R. [4.1]. It can be clearly observed that the characteristics peaks of Ni_3Fe_1 LDH is significantly broadened, and the intensity of peaks decreases suggesting less crystallinity and more defects in the stacked structure [151, 157, 158].

4.1.2 Morphological Analysis

The morphology of the LDH structures were analyzed by scanning electron microscope (SEM). Figure 4.2 displays SEM-images of Ni_3Fe_1, Ni_2Fe_1, Ni_1Fe_1 and Ni_1Fe_2 LDH structures and confirms the growth of densely packed thin sheets on nickel foil at various ratios.

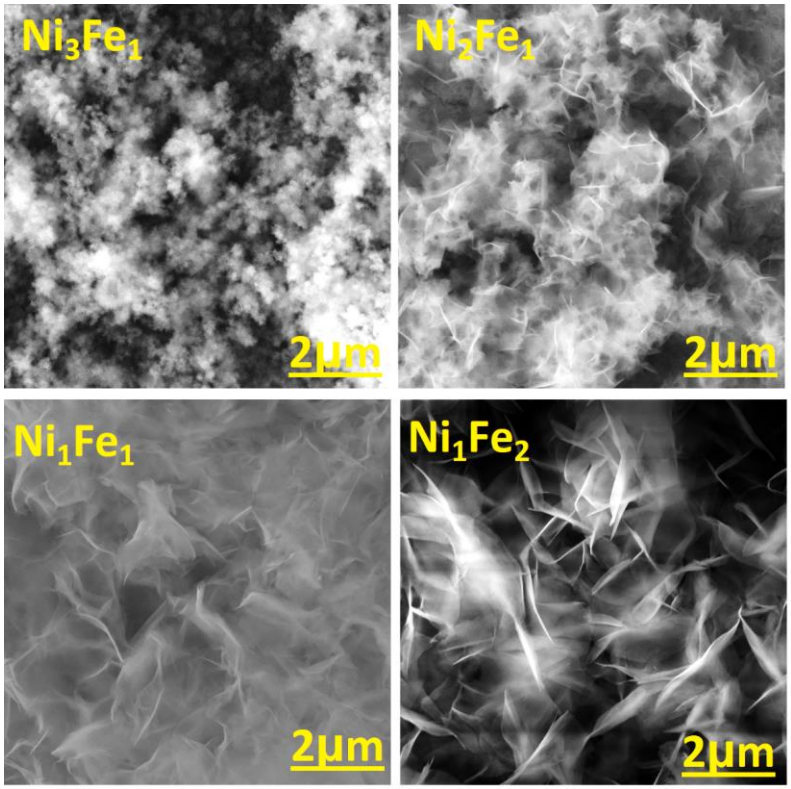

Figure 4- 2 SEM images at 2um of (a) Ni_3Fe_1, (b) Ni_2Fe_1, (c) Ni_1Fe_1, and (d) Ni_1Fe_2

The resulting film has a compact and continuous morphology observed in each of the samples. It can clearly observe that the edges of sheet-like nanocrystals forming the interlaced assemblies on the substrate.

SEM images (Fig. 4.2) show the Ni-Fe LDHs formed on the Ni foil exhibit a 3D porous structure. The Ni-Fe LDH plates with lateral sizes of several hundred nanometers are interconnected. Fig.4.2 (a) shows the morphology of Ni_3Fe_1 LDH form on the Ni foil. As observed the product shows the thin nanosheets which are intersecting each other with void spaces and play a significant role in electrochemical process because they increase the charge transfer rate during the electrochemical reactions. As the Ni and Fe ratio change, the size of the nanosheets starts increases as shown in Fig.4.3 (b-c) and has conventional porous morphology on Ni foil. These are perpendicularly in a very dense way across the substrate.

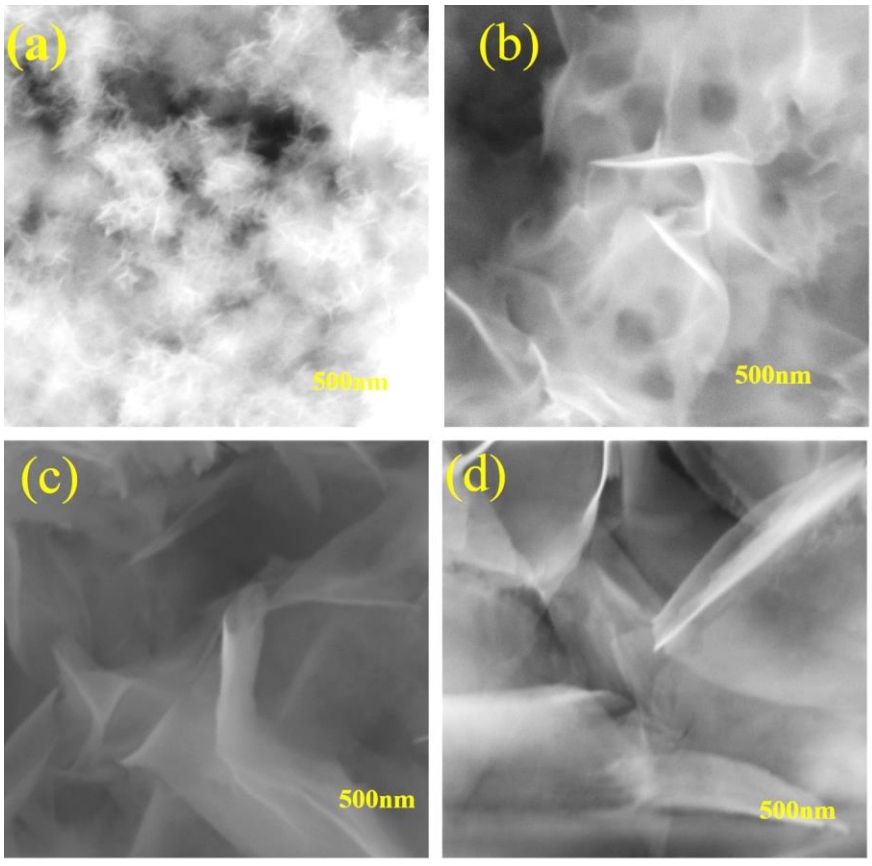

Figure 4- 3 SEM images at 500nm of (a) Ni_3Fe_1, (b) Ni_2Fe_1, (c) Ni_1Fe_1, & (d) Ni_1Fe_2

Figure 4.3 shows the magnified SEM images of the LDHs. The uniform attachment of Ni-Fe LDH onto the surface of the nickel foil efficiently avoids packing and self-aggregation. The heterostructure composite may provide a large specific surface area with porous characteristics, allowing electrolyte to flow towards whole nanosheets and therefore achieve excellent catalytic performance. Ni_1Fe_2 composite has a petal-like structure, similar to hydrangea, with an average diameter of one micron. There are many cracks between each petals, which provide different pathways for electrolyte ion penetration and mass transfer.

4.1.3 Elemental compositional analysis

Energy-dispersive x-ray spectroscopy (EDX or EDS) was employed to analyze the elemental composition of all LDHs. Samples were exposed to X-ray radiations in order to identify the elements contained by each LDH.

4.1.3.1 EDX of Ni_3Fe_1

Figure 4.4 shows the SEM and the corresponding EDX spectrum of Ni_3Fe_1 LDH. As can be seen the spectrum consists of Ni, Fe and O peaks and verify in the formation of Ni-Fe LDH. Also, the fact that the proportion of Ni, which corresponds to the substrate, is much higher than the percentage of Fe demonstrates that the coating thickness of the formed LDH is quite low. The quantitative analysis further demonstrates that the elements of the synthesized LDH are equally distributed throughout the structure.

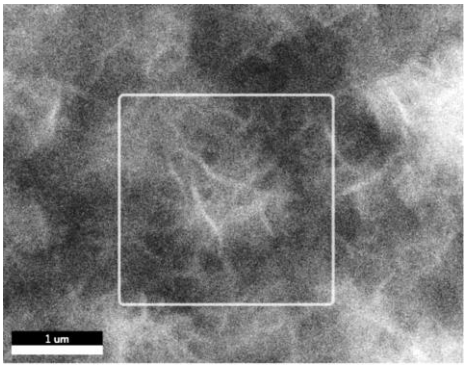

(a)

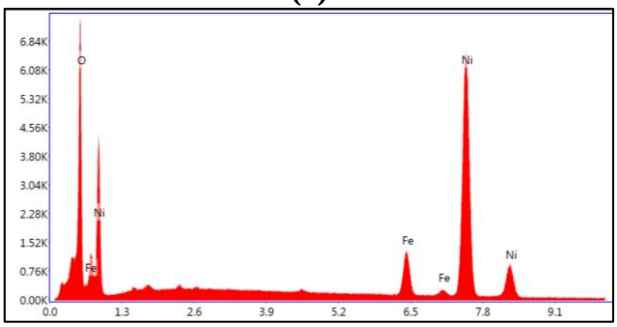

(b)

Figure 4- 4 (a) Selected EDX test location, (b) EDX Spectrum at test location

Table 4- 1 Elemental Analysis of Ni_3Fe_1

Element	Weight %	Atomic %	Net Int.	Error %	Kratio
O K	18.73	45.71	846.70	7.27	0.0900
FeK	6.63	4.64	310.80	5.11	0.0909
NiK	74.64	49.65	1871.10	2.01	0.7284

The EDS spectrum of Ni_3Fe_1-LDH also demonstrate that electrode was successfully synthesized, with the weight percentages of Ni, Fe and O in 74.64%, 6.63% and 18.73% respectively and atomic percentages of Ni, Fe and O are 49.65%, 4.64% & 45.71% respectively.

4.1.3.2 EDX of Ni_2Fe_1

Figure 4.5 shows the SEM and the corresponding EDX spectrum of Ni_2Fe_1 LDH. As can be seen in the spectrum below, edx results verify that Ni and Fe may be found in Ni-Fe LDH. Also, the fact that the proportion of Ni, which corresponds to the substrate, is much higher than the percentage of Fe demonstrates that the coating thickness of the formed LDH is quite low. The findings demonstrated that the elements of the synthesized electrode were equally distributed and spatially close to one another.

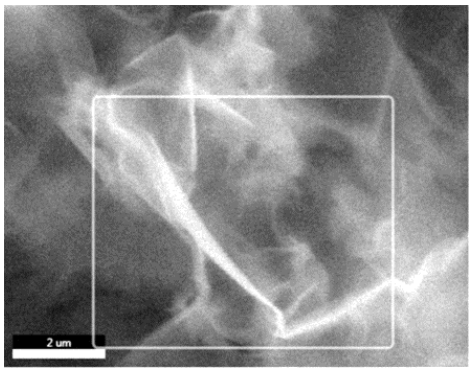

(a)

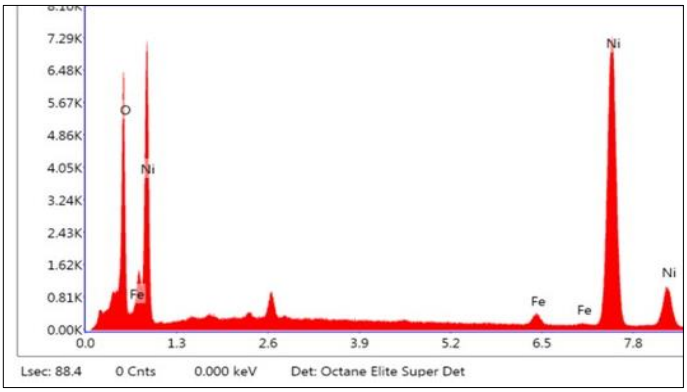

(b)

Figure 4- 5 (a) Selected EDX test location, (b) EDX Spectrum at test location

Table 4- 2 Elemental Analysis of Ni_2Fe_1

Element	Weight %	Atomic %	Net Int.	Error %	Kratio
O K	15.95	41.03	840.70	7.40	0.0751
FeK	1.54	1.13	95.70	9.59	0.0238
NiK	82.51	57.84	2468.20	1.94	0.8161

The EDS spectrum of Ni_3Fe_1-LDH also demonstrate that electrode was successfully synthesized, with the weight percentages of Ni, Fe and O in 82.51%, 1.54% and 15.95% respectively and atomic percentages of Ni, Fe and O are 57.84%, 1.13% & 41.03% respectively.

4.1.3.3 EDX of Ni_1Fe_1

Figure 4.6 shows the SEM and the corresponding EDX spectrum of Ni_1Fe_1 LDH. As can be seen in the spectrum below, edx results verify that Ni and Fe may be found in Ni-Fe LDH. Also, the fact that the proportion of Ni, which corresponds to the substrate, is much higher than the percentage of Fe demonstrates that the coating thickness of the formed LDH is quite low. The findings demonstrated that the elements of the synthesized electrode were equally distributed and spatially close to one another.

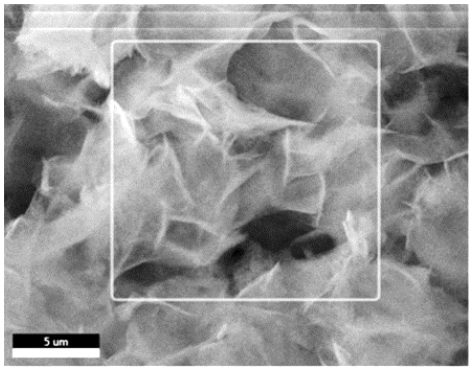

(a)

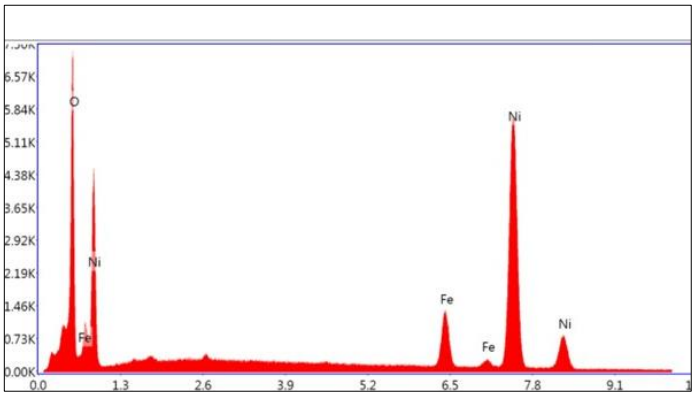

(b)

Figure 4- 6 (a) Selected EDX test location, (b) EDX Spectrum at test location

Table 4- 3 Elemental Analysis of Ni_1Fe_1

Element	Weight %	Atomic %	Net Int.	Error %	Kratio
O K	19.34	46.68	823.00	7.24	0.0937
FeK	8.08	5.59	343.30	4.75	0.1078
NiK	72.58	47.73	1688.70	2.04	0.7059

The EDS spectrum of Ni_1Fe_1-LDH also demonstrate that electrode was successfully synthesized, with the weight percentages of Ni, Fe and O in 71.58%, 8.08% and 19.34% respectively and atomic percentages of Ni, Fe and O are 47.73%, 5.59% & 46.68% respectively.

4.1.3.4 EDX of Ni_1Fe_2

Figure 4.7 shows the SEM and the corresponding EDX spectrum of Ni_1Fe_1 LDH. As can be seen in the spectrum below, edx results verify that Ni and Fe may be found in Ni-Fe LDH. Also, the fact that the proportion of Ni, which corresponds to the substrate, is much higher than the percentage of Fe demonstrates that the coating thickness of the formed LDH is quite low. The findings demonstrated that the elements of the synthesized electrode were equally distributed and spatially close to one another.

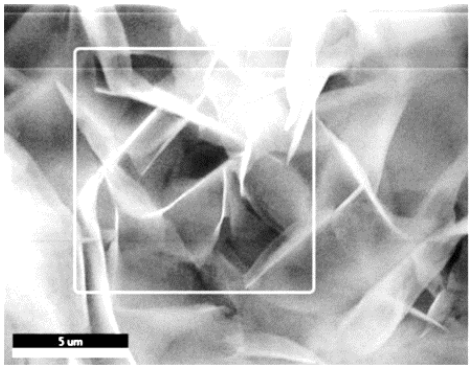

(a)

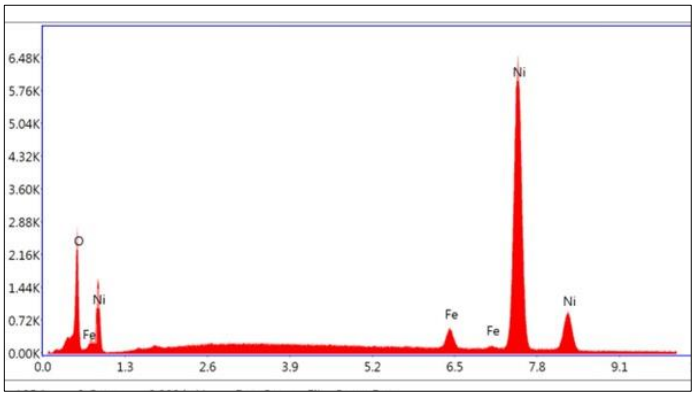

(b)

Figure 4- 7 (a) Selected EDX test location, (b) EDX Spectrum at test location

Table 4- 4 Elemental Analysis of Ni_1Fe_2

Element	Weight %	Atomic %	Net Int.	Error %	Kratio
O K	8.00	24.15	269.50	7.96	0.0363
FeK	3.05	2.64	124.90	7.25	0.0468
NiK	88.95	73.20	1796.70	1.96	0.8958

The EDS spectrum of Ni_1Fe_1-LDH also demonstrate that electrode was successfully synthesized, with the weight percentages of Ni, Fe and O in 88.95%, 3.05% and 8% respectively and atomic percentages of Ni, Fe and O are 73.20%, 2.64% & 24.15% respectively.

4.1.4 Fourier Transform Infrared Spectroscopy (FTIR)

In order to further analyze the structural features of LDHs Fourier Transform-infrared (FT-IR) analysis was performed as shown in Figure 4.8 to learn more about the composite's underlying structural features. The ion penetration and mass transport properties of an electrolyte were studied using FT-IR.

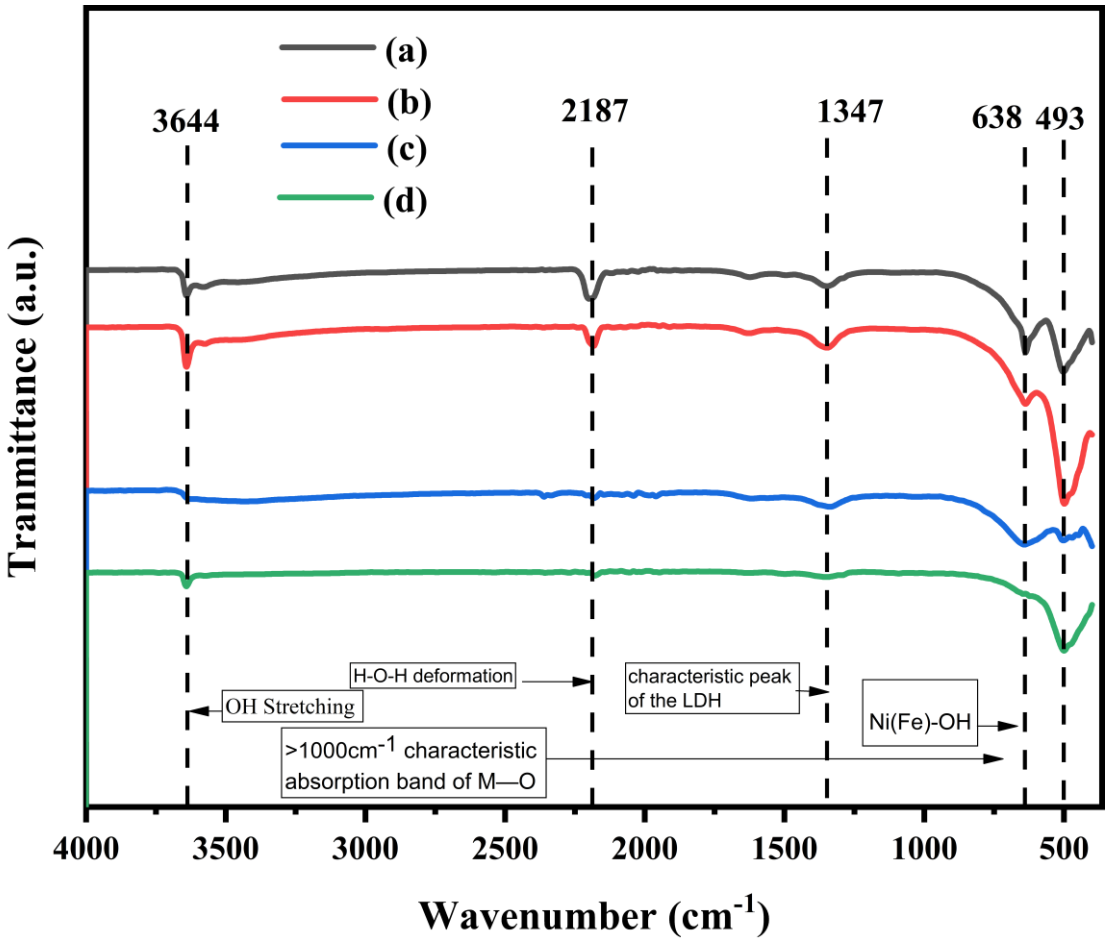

Figure 4- 8 FTIR spectra of (a) Ni_3Fe_1, (b) Ni_2Fe_1, (c) Ni_1Fe_1 & (d) Ni_1Fe_2

The FTIR spectra, show a prominent band at 1347 cm^{-1}, substantiate the hypothesis that CO_3^{2-} is present in the LDH samples. Two bands, one at 3650 cm^{-1} corresponding to O-H

stretching and the other at 2187 cm^{-1} corresponding to H-O-H deformation, provide qualitative evidence that the LDH samples have been hydrated. Bands with a frequency lower than 1000 cm^{-1} relate to the bonds that create the hydroxide layers between oxygen and metallic atoms [4.2].

4.2 Electrochemical Measurements:

4.2.1 Cyclic voltammetry:

Cyclic voltammetry tests were performed of all the Ni-Fe LDHs prepared with different molar ratio under the same condition. The polarization curve of each electrode was analyzed in 1M KOH at potential window 1 to 2.2 vs. RHE using a Silver-Silver Chloride electrode as a reference electrode at 5 $mVsec^{-1}$. Platinum wire was used as a counter electrode. The polarization curves are quite similar to one another, however, as can be seen in fig 4.9, Ni_3Fe_1 showed the most considerable results among all the samples, with the highest current density and the least amount of overpotential. Ni_2Fe_1, Ni_1Fe_1 and Ni_1Fe_2 also displayed better results but less than Ni_3Fe_1. Here we have used bare nickel foil as a reference only. The Ni-Foil have shown comparatively poor response. At the start material oxidation peak is observed due to oxidation of nickel Ni^{+2} into Ni^{+3}. Owing to this material own oxidation peaks, over potential was calculated using the reverse linear sweep voltammetry scan of cyclic voltammetry in which there is no material oxidation peak to avoid the uncertainties is noted. All the cyclic voltammetry curve shows a distorted rectangular shape curves at lower scan rates, which shows that the materials can store the charges on surface as well electrode-electrolyte interface, hence conforming electrical double layer capacitance.

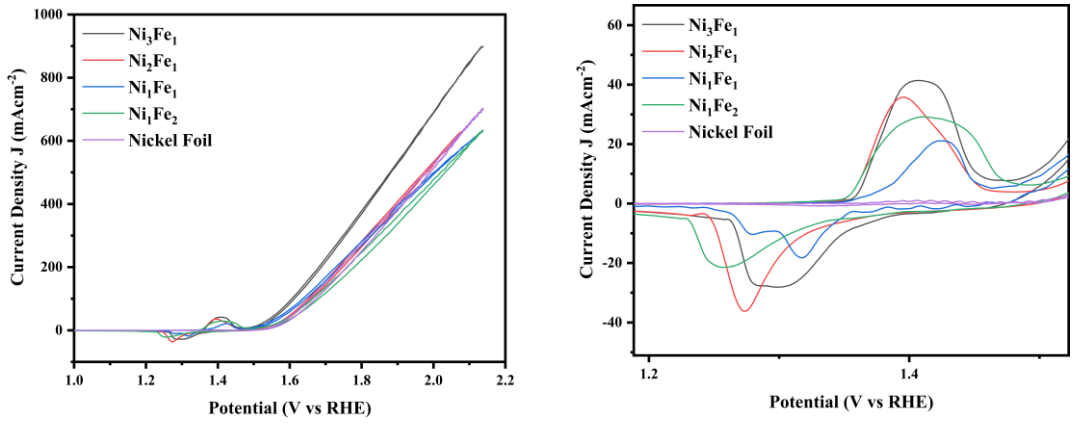

(a) **(b)**

Figure 4- 9 Comparison of Ni_3Fe_1, Ni_2Fe_1, Ni_1Fe_1, Ni_1Fe_2 and Ni-Foil at 5 mV s^{-1} in 1M KOH (a) CVs curves (b) Magnified region of CV curves graph

Fig. 4.10 (a-d) shows the cyclic voltammogram of Ni_3Fe_1, Ni_2Fe_1, Ni_1Fe_1, & Ni_1Fe_2 at various scan rates between 5 and 100 mVs^{-1} of applied potential. Clear redox peaks (corresponding to B-type curves) can be seen in the potential range of 1-1.65 (V vs RHE) [184]. Every single CV curve can be interpreted as a pair of redox peaks.

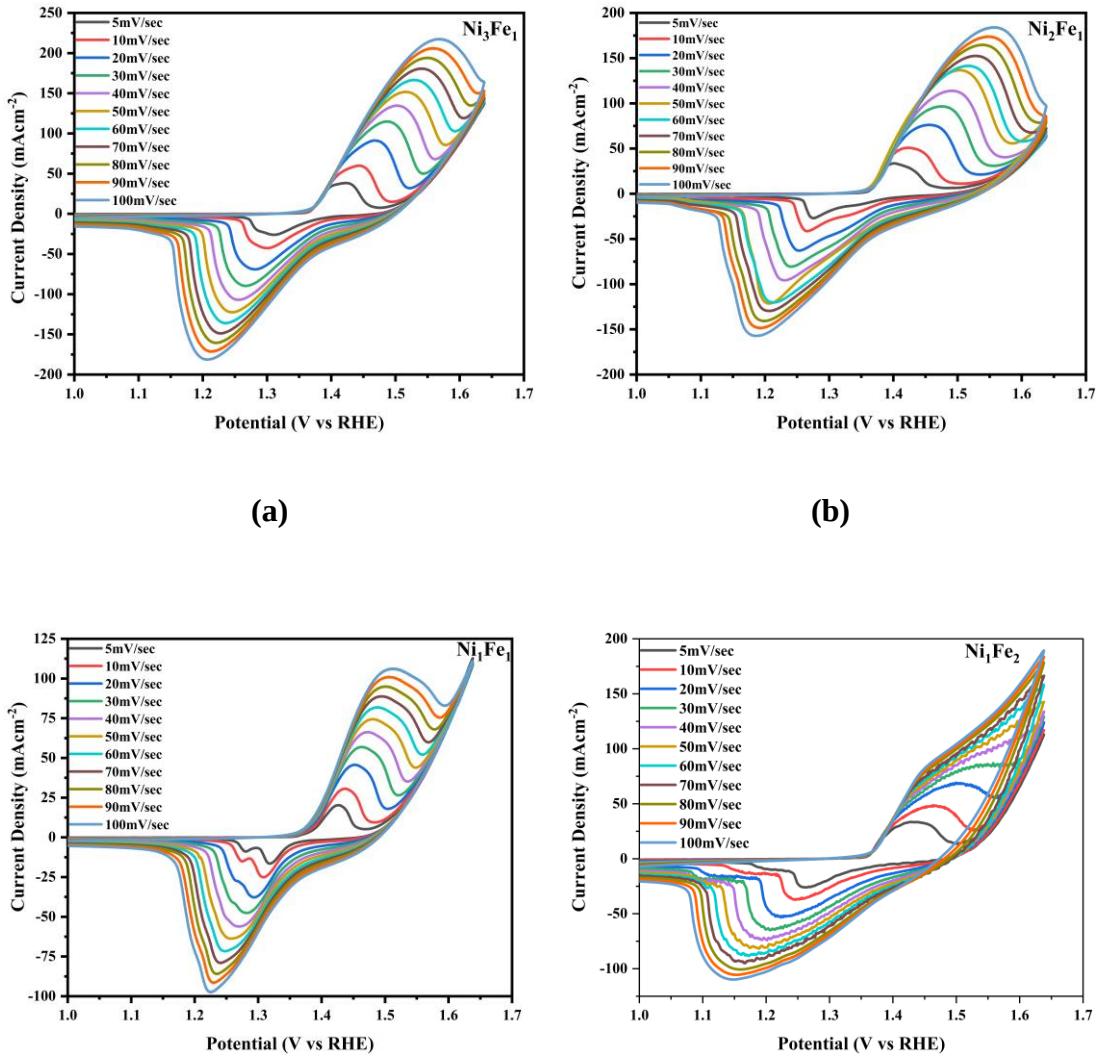

Figure 4- 10 CV curves at scan rate 5,10 ,20 ,30 ,40 ,50 ,60 ,70 ,80, 90 & 100 mV/sec of (a) Ni_3Fe_1, (b) Ni_2Fe_1, (c) Ni_1Fe_1, & (d) Ni_1Fe_2

The highest current density has been observed for Ni_3Fe_1. The forward scan results in oxidation of catalyst for oxides and conducting removal of electrons, while the reverse scan undergoes reduction of Ni_3Fe_1 catalyst in a reversible manner. The adsorption of OH^- at the electrode surface is the key mechanism that determines the reversibility of the electrode material. The CV curves do not change as the scan rate is raised, demonstrating

the excellent cyclic stability, low resistance, and good electrocatalytic efficiency of all catalysts. Increasing the scan rate causes the absorbers layer's impedance to decrease, leading to a high current density. The redox activity is localized to the surface of the synthesized electrode as the number of redox peaks increases with increasing scan rates, demonstrating the catalyst's stability.

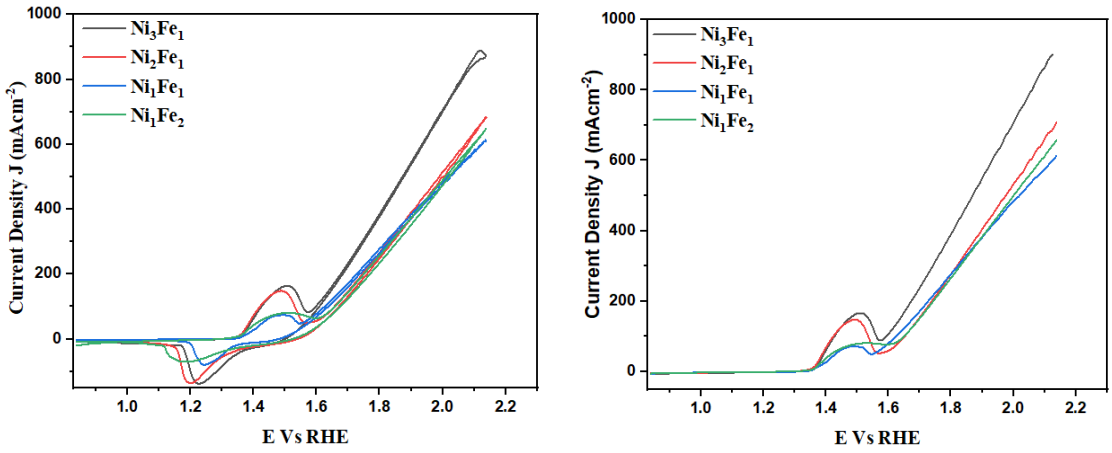

Figure 4- 11 Polarization Curves (a) CVs (b) LSVs of Ni_3Fe_1, Ni_2Fe_1, Ni_1Fe_1, and Ni_1Fe_2 at 50 mV s^{-1} in 1M KOH

Figure 4.11 Shows similar trend as described earlier when scan rate is increased to 50 mV/sec. Ni_3Fe_1-LDH showed the most considerable results among all the samples, with the highest current density and the least amount of overpotential.

4.2.2 Linear sweep voltammetry:

The synthesized catalysts OER performances were evaluated by LSV polarizations using a three-electrode assembly consisting of silver-silver chloride, platinum wire, and synthesized electrocatalysts (Ni_3Fe_1, Ni_2Fe_1, Ni_1Fe_1, Ni_1Fe_2, and Ni-foil) in a 1M KOH solution. Here we have used bare nickel foil as a reference only. The polarization curve of each electrode was analyzed in 1M KOH at potential window 1 to 2.2 vs. RHE using a Silver-Silver Chloride as a reference electrode at 5 $mVsec^{-1}$.

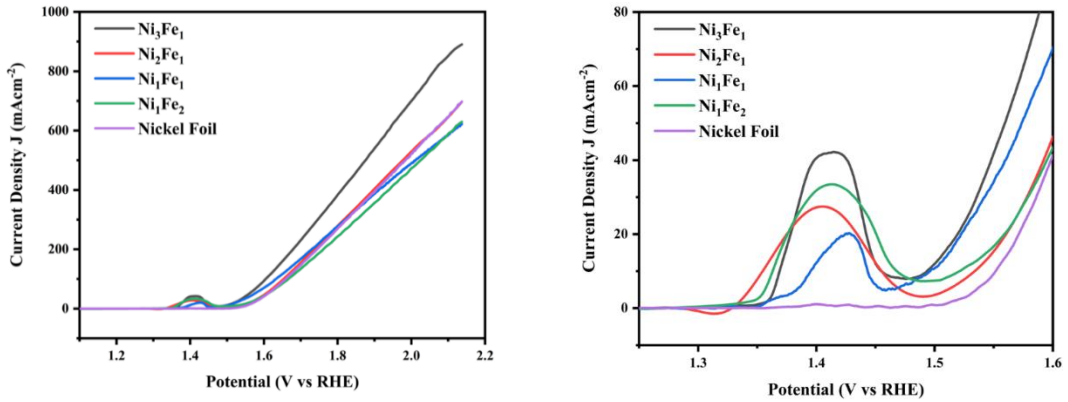

Figure 4- 12 Comparison of Ni_3Fe_1, Ni_2Fe_1, Ni_1Fe_1, Ni_1Fe_2 and Ni-Foil at 5 mV s^{-1} in 1M KOH (a) LSV curves (b) Magnified region of LSV curves graph

Figure 4.12 demonstrates the polarization curves of all electrodes. Ni_3Fe_1-LDH showed the most considerable results among all the electrodes, with the highest current density and the least amount of overpotential. In comparison to the all electrodes, Ni_3Fe_1 LDH had the highest current density, measuring 890 $mAcm^{-2}$, and the lowest overpotential measuring 264.3 mV.

4.2.3 Overpotential:

Overpotential is also considered when assessing electrochemical activity. The overpotential values are shown in Figure 4.13 when the current density is 10 $mAcm^{-2}$. Overpotentials ranged from 264.3 to 322.3 millivolts as measured by the instrument (mV). It is essential to keep in mind that in-situ synthesized electrodes by hydrothermal method were used in this experiment, and no conductive carbon material was added. The lowest overpotential was of Ni_3Fe_1 (264.3 mV) at current density of 10 mA cm^{-2}. The benchmark Ni-Foil demonstrate weaker OER activity as its overpotential was 322.3 mV at current density of 10 mA cm^{-2}.

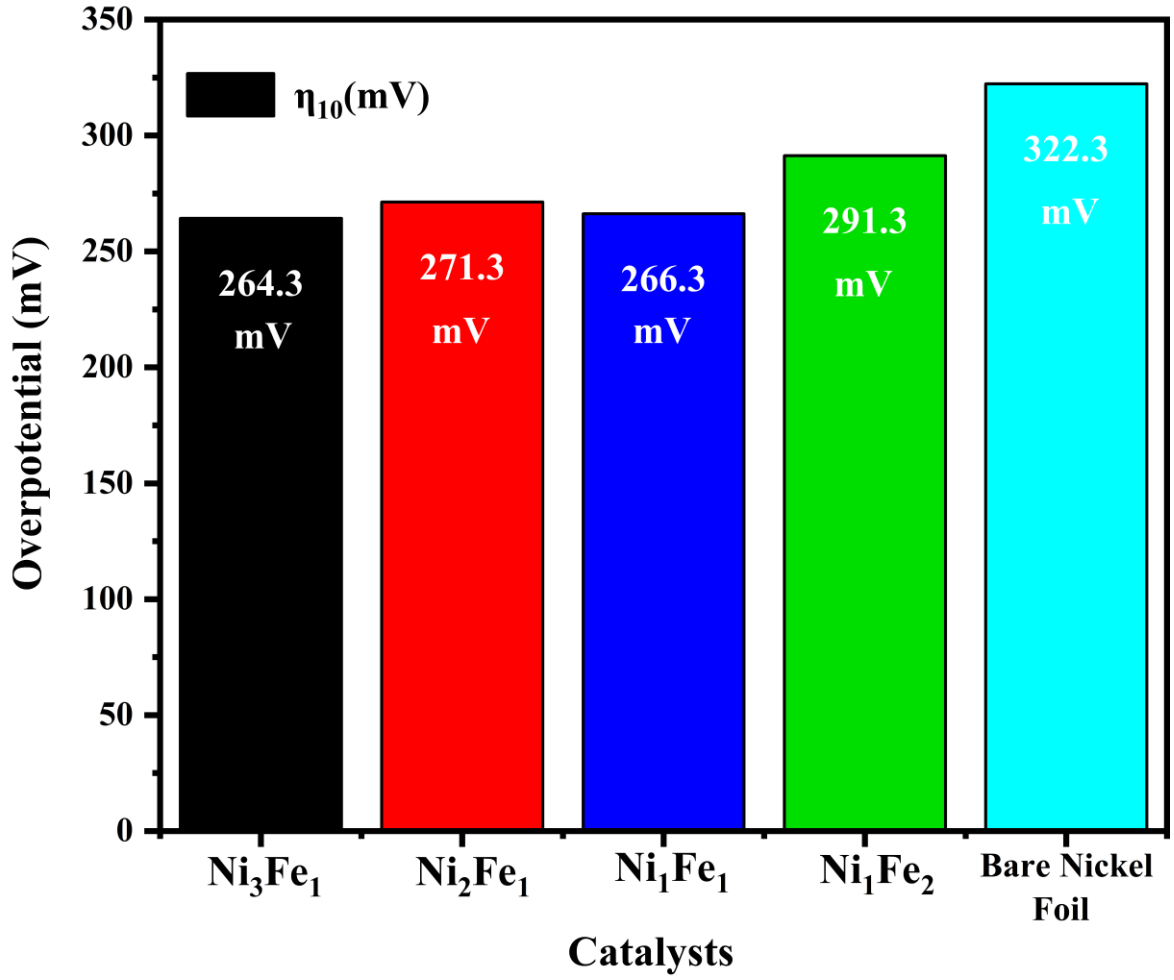

Figure 4- 13 Comparison of Overpotentials at Current Density of 10 $mAsec^{-2}$ of Ni_3Fe_1, Ni_2Fe_1, Ni_1Fe_1, Ni_1Fe_2 LDHs & Bare Ni-Foil

In addition, the purpose of the research presented in this project is to compare samples that were collected under identical conditions. This is because a comparison with the materials presented in other publications that also use the overpotential is not accurate due to the large number of experimental factors that have the potential to influence the findings.

4.2.4 Tafel Analysis

For oxygen Evolution process, a catalyst should operate at low potential range, and given high current and maximum stability and durability. Accordingly, Tafel plots of all the as-prepared samples were calculated within the linear regions fitted into the Tafel equation ($\eta = b\log J + a$) where b is Tafel slope. All the catalyst prepared at different time displayed

higher kinetics with lower Tafel slope values. Well-balanced kinetic during catalysis is an indication of a small Tafel slope value. However, the best Ni_3Fe_1 exhibited much lower value with only 32 mV dec^{-1} and other candidates shows such as Ni_2Fe_1 (46 $mVdec^{-1}$), Ni_1Fe_1 (47 $mVdec^{-1}$), and Ni_1Fe_1 (61 $mVdec^{-1}$). Tafel slopes are given in fig 4.14.

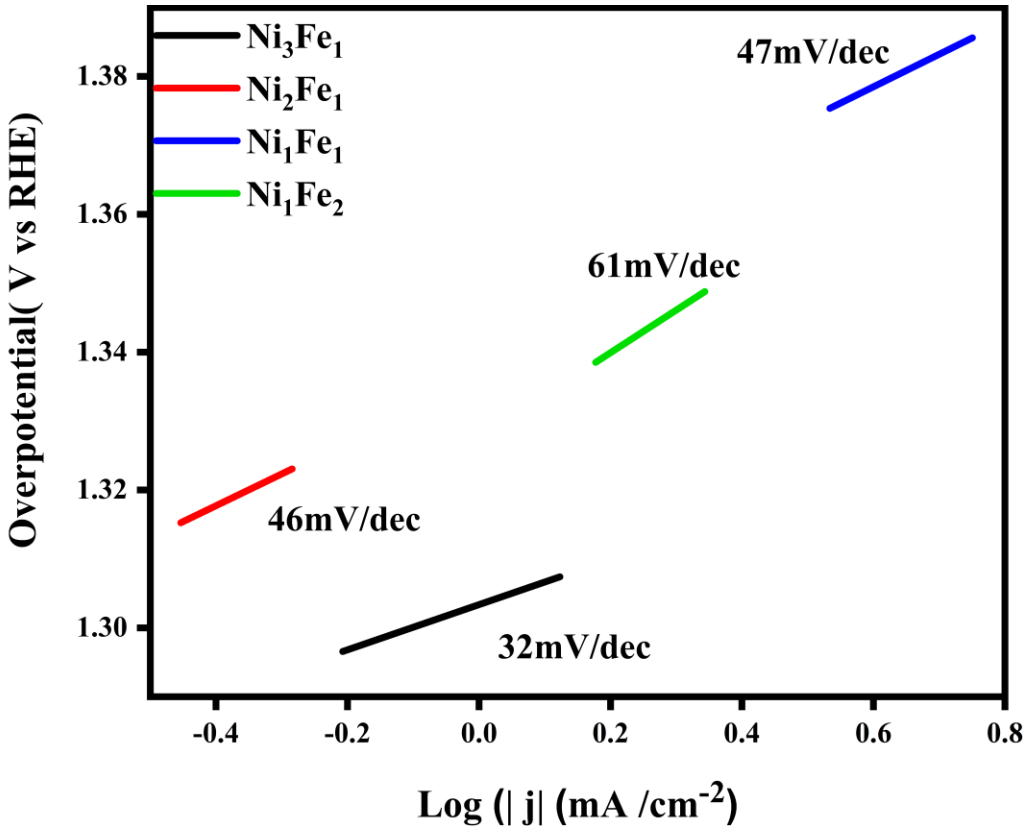

Figure 4- 14 Tafel Slope of Ni_3Fe_1, Ni_2Fe_1, Ni_1Fe_1, and Ni_1Fe_2

4.2.5 Electrochemical Impedance Spectroscopy

To study the reaction kinetics of all the prepared electrodes, electrochemical impedance spectroscopy was performed. The test is carried out in 1M KOH solution over a frequency range of 0.1 to 100kHz. Fresh electrolyte was employed for all the results to minimize the difference in solution resistance. The fig 4.15 shows the respective Nyquist EIS plots of all the samples as synthesized. Solution resistance, Rs, is the resistance of the electrolyte and R_{ct} is the charge transfer resistance which is the inter-facial resistance between the material and the electrolyte. The latter is the resistance which indicates the kinetics of

charge transfer in the process of oxygen evolution reaction OER. Furthermore, Fig 4.15 demonstrates that an increase in voltage results in a considerable reduction in the charge transport resistance.

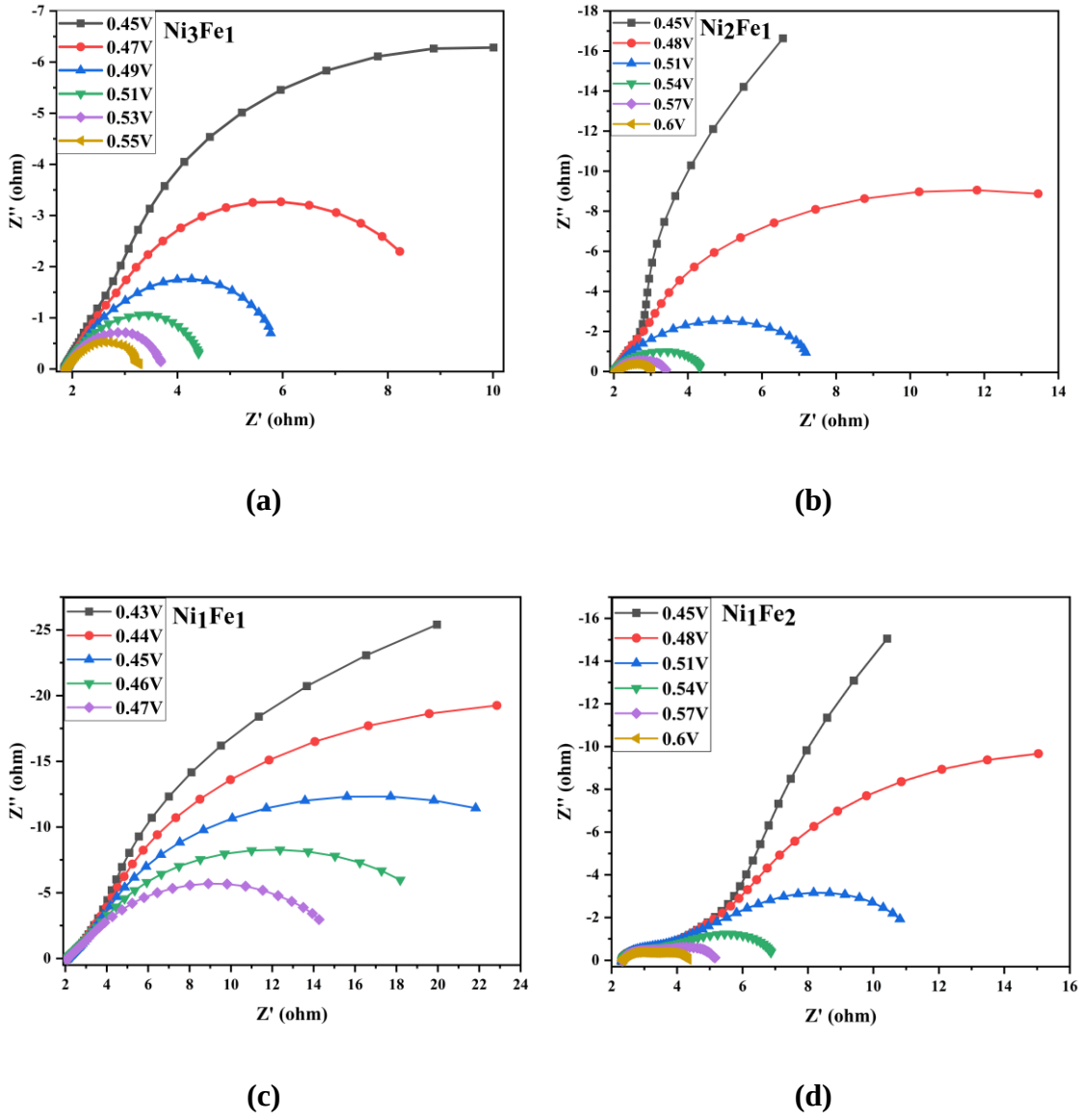

Figure 4- 15 Electrostatic Impedance Spectroscopy (a) Ni_3Fe_1, (b) Ni_2Fe_1, (c) Ni_1Fe_1, and (d) Ni_1Fe_2 in 1M KOH

To compare the reaction kinetics, the EIS curves at 0.45V were plotted. Figure 4.16 shows that the catalyst Ni_3Fe_1 has least charge transfer resistance and reflected higher kinetics comparatively. This was in good accordance with the cyclic and linear sweep voltammetry

results, SEM and XRD analysis. Ni_3Fe_1 has a smaller semicircle, implying its charge transfer resistance is lower.

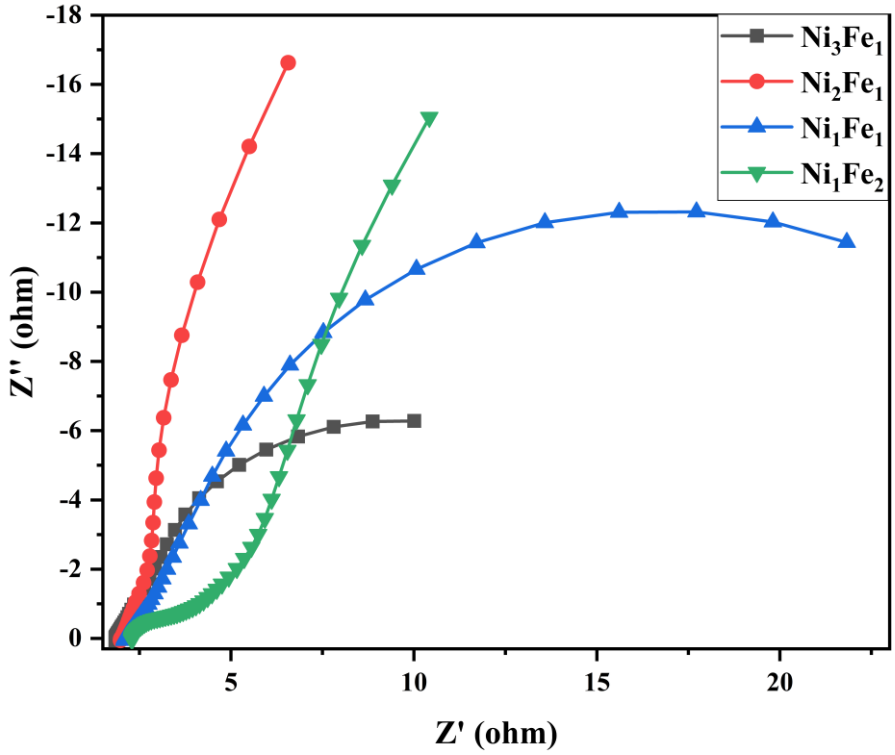

Figure 4- 16 Comparison of Electrostatic Impedance Spectroscopy of Ni_3Fe_1, Ni_2Fe_1, Ni_1Fe_1, and Ni_1Fe_2 at 0.45V

4.2.6 Stability Test

For industrial application and commercialization and of the catalyst, long term stability is immensely important. Durability of the materials are checked by employing numerous methods. Among them, repetitive linear sweep voltammetry scans, chrono-potentiometric and chronoamperometric scans at different value of voltage and current are frequently evaluated. Long-term catalytic testing for OER of the best sample demonstrate an exceptionally high stability of electrocatalysts for water oxidation at modest electrochemical conditions. Under constant current densities of $10mAcm^{-2}$, 20 $mAcm^{-2}$ and 50 $mAcm^{-2}$, Ni_3Fe_1 electrode sustain potential values for OER in a very hostile oxidative environment (fig 4.17).

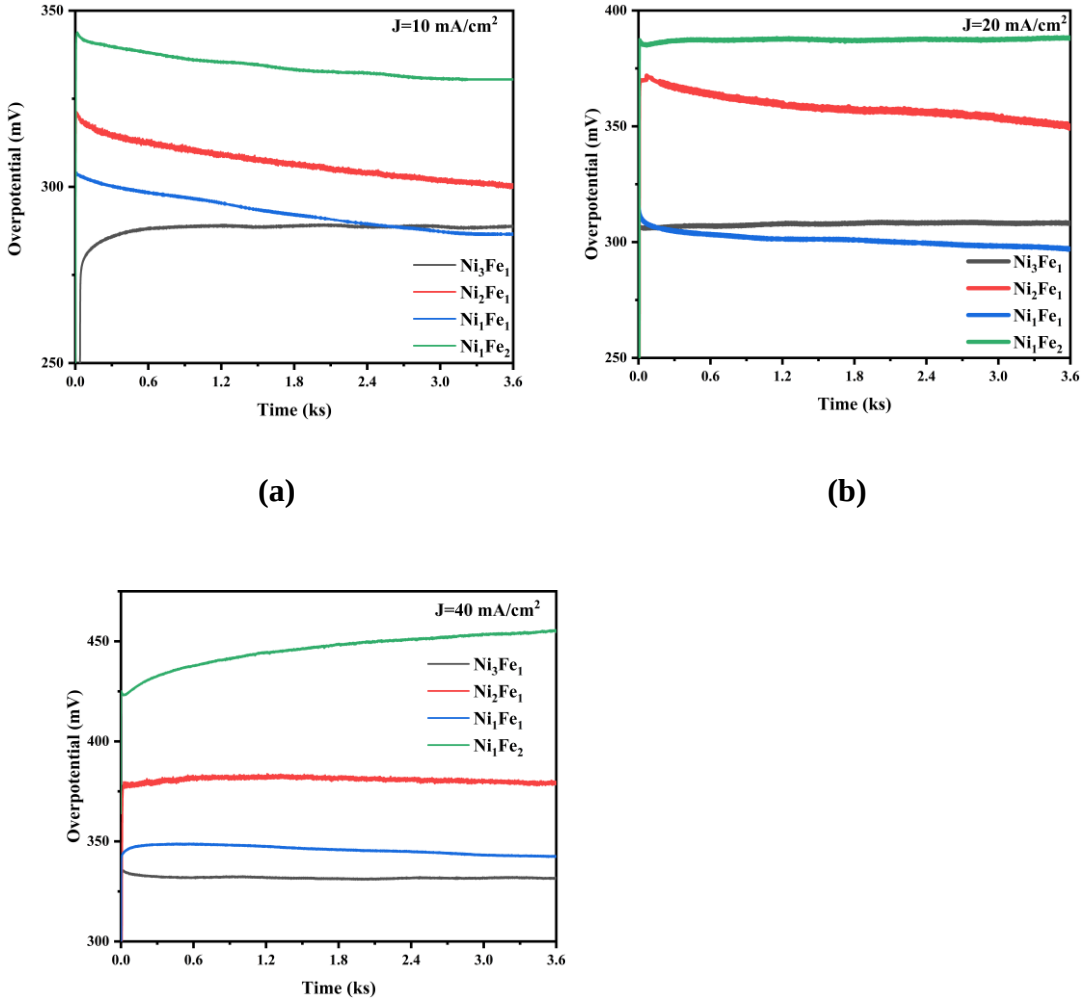

Figure 4- 17 Chronopotentiometry Tests of Ni_3Fe_1, Ni_2Fe_1, Ni_1Fe_1, Ni_1Fe_2 at (a) 10, (b) 20, (c) 40 $mAcm^{-2}$

When the stability test was conducted at 10 mA cm^{-2} and 20 $mAcm^{-2}$, there was virtually no degradation. 99 percent of the catalyst was conserved. In the case of 40 $mAcm^{-2}$, however, the voltage decreased due to the oxidation of nickel on the surface of the electrode, which provides new sites for the oxygen evolution event (OER).

In addition to the Chronopotentiometry Test, the stability was verified by taking LSVs before and after the stability test. (Fig. 4.18 a-d). Ni_3Fe_1 current density was discovered to be close to its starting value. As a result, Ni_3Fe_1 catalyst is sufficiently stable for widespread use, as seen above.

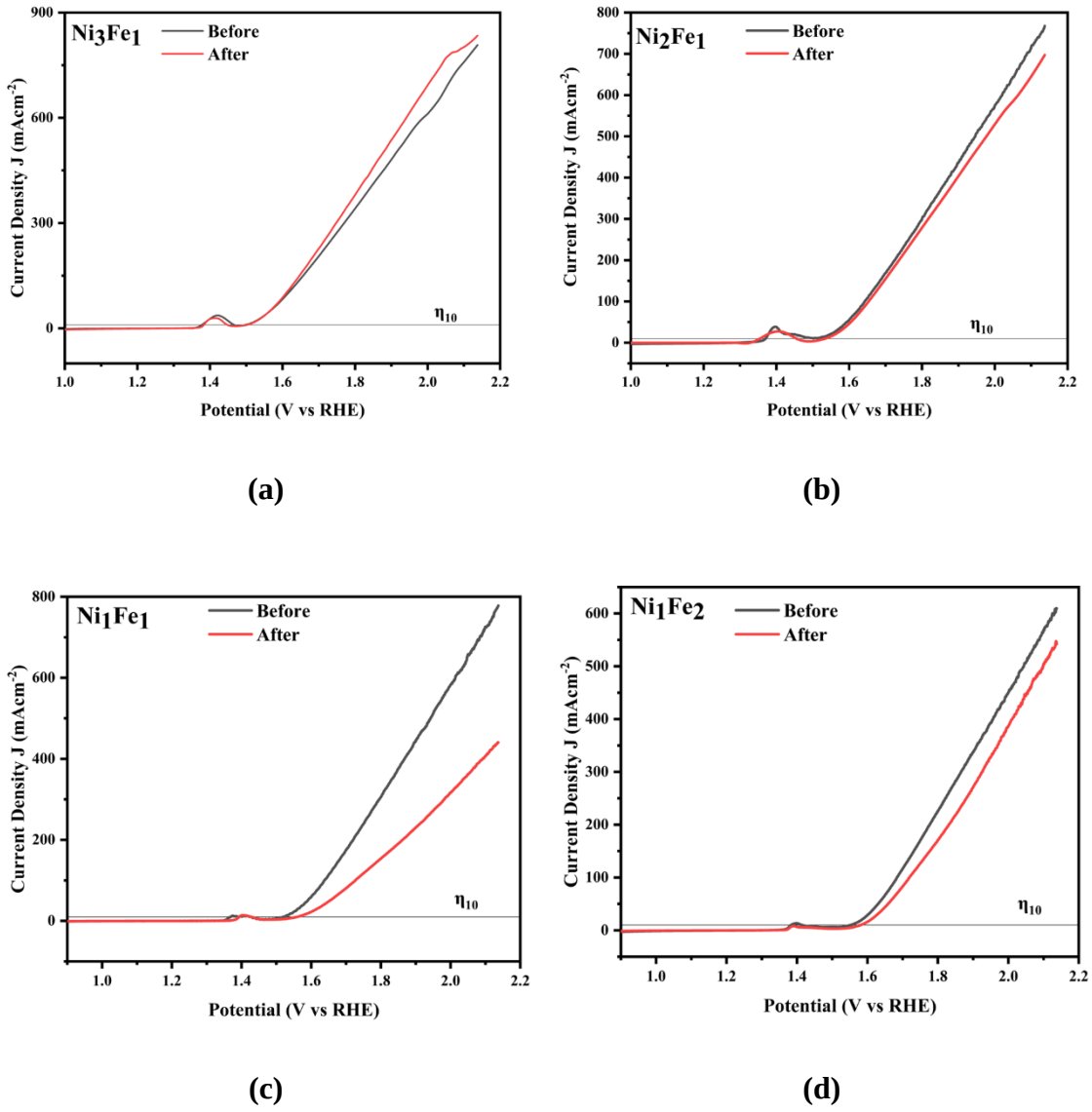

Figure 4- 18 LSV Curves of (a) Ni_3Fe_1, (b) Ni_2Fe_1, (c) Ni_1Fe_1, and (d) Ni_1Fe_2 taken before and after Chronopotentiometry Tests at 5 mV/sec in 1M KOH

LSV polarization curves were used to measure the overpotential of each catalyst before and after the stability test, as illustrated in Figure 4.19. This experiment demonstrates conclusively that Ni_3Fe_1 virtually loses its overpotential compared to other electrodes at a current density of 10 $mAcm^{-2}$.

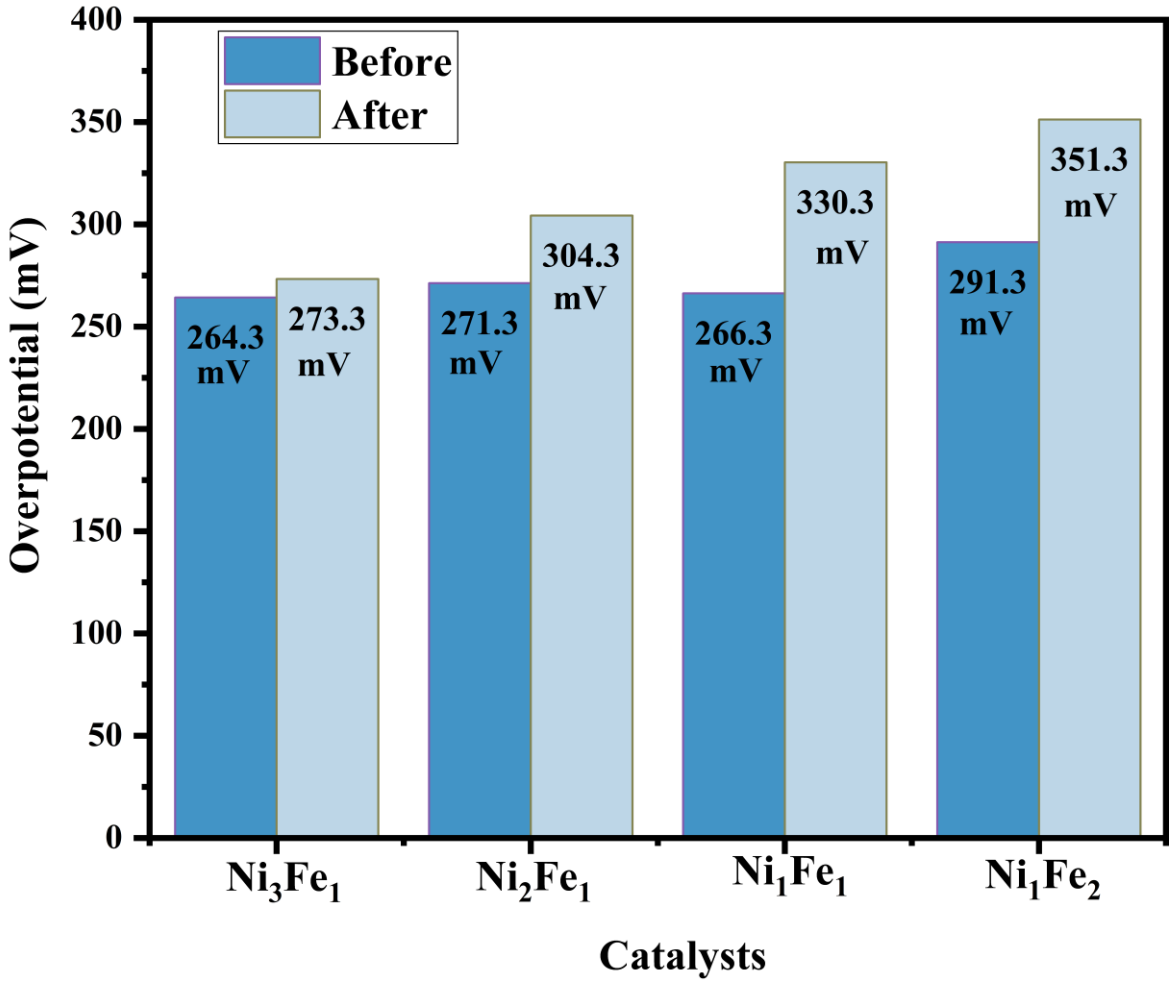

Figure 4- 19 Comparison of Overpotentials before & after chronopotentiometry tests of Ni_3Fe_1, Ni_2Fe_1, Ni_1Fe_1, Ni_1Fe_2 at 10mAcm^{-2} in 1M KOH

Conclusion

The study in the thesis delves deeply into the recent advancements made in Ni-Fe LDH as an electrocatalyst for HER & OER. Study's primary objective is to identify a cheap, non-precious-metal catalyst and conductive substrate exhibiting good catalytic activity and stability. Although significant attention has been paid to Nickel foam as a conductive substrate, very few works use Nickel foil. There was still space for further research, to that end, we offered a dynamic approach we synthesized four Ni-Fe LDH (Ni_3Fe_1, Ni_2Fe_1, Ni_1Fe_1, Ni_1Fe_2) grew hydrothermally on nickel foil in a direct growth process and studied the importance of the molar ratio of the salts on structural, morphological, and electrochemical properties. The results given here reveal that the layered double hydroxides (Ni_3Fe_1) synthesized in this work have a reduced overpotential (264.3 mV), higher current density (890 mA cm^{-2}), lower Tafel slope (32 mV dec^{-1}) and higher stability, providing further support for the ongoing research of LDHs for application as Ni-Fe electrocatalysts. In Sample comparisons within the same group, we see that a higher Ni/Fe ratio is associated with significantly broader XRD peaks, and the intensity of peaks decreases suggesting less crystallinity and more defects in the stacked structure values. A larger concentration of Ni is reported to be unfavorable for the catalyst's efficiency in many sources [8,9,13], suggesting that lower Ni/Fe ratios (1.5, 2, and 0.8 correspondingly) are optimal. However, our research shows that slight variations in composition and structure do not lead to appreciable variations in electrocatalytic performance. This study presents a unique approach to the development of Ni-Fe LDHs for use in the OER catalysis. We look at how the Ni/Fe atomic ratio and crystallinity of the synthesized material affect the electrocatalytic activity of Ni/Fe LDH. Finally, this study adds to our understanding of the structure and Ni/Fe ratio, two factors crucial to the advancement of Ni-Fe LDHs. In further research, other catalyst supports could be used to increase catalyst loading, and the material will be tested in more realistic settings.

References

[1] Dell, Ronald M., and David Anthony James Rand. "Energy storage a key technology for global energy sustainability." Journal of power sources 100, no. 1-2 (2001): 2-17.

[2] Jacobson, Mark Z. "Review of solutions to global warming, air pollution, and energy security." Energy and Environmental Science 2, no. 2 (2009): 148-173.

[3] Lewis, Nathan S., and Daniel G. Nocera. "Powering the planet: Chemical challenges in solar energy utilization." Proceedings of the National Academy of Sciences 103, no. 43 (2006): 15729-15735.

[4] Lewis, Nathan S., George Crabtree, Arthur J. Nozik, Michael R. Wasielewski, Paul Alivisatos, Harriet Kung, J. Tsao et al. Basic Research Needs for Solar Energy Utilization. Report of the Basic Energy Sciences Workshop on Solar Energy Utilization, April 18-21, 2005. DOESC (USDOE Office of Science (SC)), 2005.

[5] Kim, Seongyul, Nikhil Koratkar, Tansel Karabacak, and Toh-Ming Lu. "Water electrolysis activated by Ru nanorod array electrodes." Applied physics letters 88, no. 26 (2006): 263106.

[6] Dresselhaus, M. SêOn, and I. L. Thomas. "Alternative energy technologies." Nature 414, no. 6861 (2001): 332-337.

[7] Hoegh-Guldberg, Ove, Daniela Jacob, M. Bindi, S. Brown, I. Camilloni, A. Diedhiou, R. Djalante et al. "Impacts of 1.5 C global warming on natural and human systems." Global warming of 1.5Âr C. An IPCC Special Report (2018).

[8] Halkos, George E., and Eleni-Christina Gkampoura. "Reviewing Usage, Potentials, and Limitations of Renewable Energy Sources." Energies 13, no. 11 (2020): 2906.

[9] Seh, Zhi Wei, Jakob Kibsgaard, Colin F. Dickens, I. B. Chorkendorff, Jens K. NÃÿrskov, and Thomas F. Jaramillo. "Combining theory and experiment in electrocatalysis: Insights into materials design." Science 355, no. 6321 (2017).

[10] Barber, James. "Photosynthetic energy conversion: natural and artificial." Chemical Society Reviews 38, no. 1 (2009): 185-196.

[11] Larcher, Dominique, and Jean-Marie Tarascon. "Towards greener and more sustainable batteries for electrical energy storage." Nature chemistry 7, no. 1 (2015): 19-29.

[12] Napp, Tamaryn A., Ajay Gambhir, Thomas P. Hills, Nicholas Florin, and Paul S. Fennell. "A review of the technologies, economics and policy instruments for decarbonizing energy-intensive manufacturing industries." Renewable and Sustainable Energy Reviews 30 (2014): 616-640.

[13] Ball, Michael, and Marcel Weeda. "The hydrogen economyâASvision or reality?." International Journal of Hydrogen Energy 40, no. 25 (2015): 7903-7919.

[14] Tollefson, Jeff. "Hydrogen vehicles: Fuel of the future." Nature 464, no. 7293 (2010): 1262-1264.

[15] Pilavachi, Petros A., Anatoli I. Chatzipanagi, and Antonia I. Spyropoulou. "Evaluation of hydrogen production methods using the analytic hierarchy process." International Journal of hydrogen energy 34, no. 13 (2009): 5294-5303.

[16] Turner, John A. "A realizable renewable energy future." Science 285, no. 5428 (1999): 687-689.

[17] Osterloh, Frank E. "Inorganic nanostructures for photoelectrochemical and photocatalytic water splitting." Chemical Society Reviews 42, no. 6 (2013): 2294-2320.

[18] Crabtree, George W., Mildred S. Dresselhaus, and Michelle V. Buchanan. "The hydrogen economy." Physics today 57, no. 12 (2004): 39-44.

[19] Pletcher, Derek, and Xiaohong Li. "Prospects for alkaline zero gap water electrolysers for hydrogen production." International Journal of Hydrogen Energy 36, no. 23 (2011): 15089 15104.

[20] Dincer, Ibrahim, and Canan Acar. "A review on clean energy solutions for better sustainability." International Journal of Energy Research 39, no. 5 (2015): 585- 606.

[21] Schlapbach, Louis, and Andreas ZÃ¼ttel. "Hydrogen-storage materials for mobile applications." In Materials for sustainable energy: a collection of peer-reviewed research and review articles from nature publishing group, pp. 265-270. 2011.

[22] Goodenough, John B. "Electrochemical energy storage in a sustainable modern society." Energy and Environmental Science 7, no. 1 (2014): 14-18.

[23] GÃutz, Manuel, Jonathan Lefebvre, Friedemann MÃurs, Amy McDaniel Koch, Frank Graf, Siegfried Bajohr, Rainer Reimert, and Thomas Kolb. "Renewable Power-to-Gas: A technological and economic review." Renewable energy 85 (2016): 1371-1390.

[24] Dunn, Seth. "Hydrogen futures: toward a sustainable energy system." International journal of hydrogen energy 27, no. 3 (2002): 235-264.
[25] Pivovar, Bryan. H2@ Scale Workshop Report. No. NREL/BK-5900-68244. National Renewable Energy Lab.(NREL), Golden, CO (United States), 2017.
[26] Dincer, Ibrahim, and Canan Acar. "Review and evaluation of hydrogen production methods for better sustainability." International journal of hydrogen energy 40, no. 34 (2015): 11094 11111.
[27] Aval, Leila Fekri, and Seyed Mohammad Elahi. "Hydrogen gas detection using MOS capacitor sensor based on palladium nanoparticles-gate." Electronic Materials Letters 13, no. 1 (2017): 77-85.
[28] Ramachandran, Ram, and Raghu K. Menon. "An overview of industrial uses of hydrogen." International journal of hydrogen energy 23, no. 7 (1998): 593-598.
[29] Song, Yu Guang, Bin Liu, Lan Fen Wang, Mai He Li, and Yang Liu. "Damage to the oxygen-evolving complex by superoxide anion, hydrogen peroxide, and hydroxyl radical in photoinhibition of photosystem II." Photosynthesis Research 90, no. 1 (2006): 67-78.
[30] Umena, Yasufumi, Keisuke Kawakami, Jian-Ren Shen, and Nobuo Kamiya. "Crystal structure of oxygen-evolving photosystem II at a resolution of 1.9 ÃE." Nature 473, no. 7345 (2011): 55-60.
[31] Tsui, Emily Y., Rosalie Tran, Junko Yano, and Theodor Agapie. "Redox-inactive metals modulate the reduction potential in heterometallic manganeseâASoxido clusters." Nature chemistry 5, no. 4 (2013): 293-299.
[32] McCool, N.S., et al., A Co4O4 âA.cubaneâAI water oxidation catalyst inspired by photosynthesis. Journal of the American Chemical Society, 2011. 133(30): p. 11446-11449.
[33] Zhang, M., M. De Respinis, and H. Frei, Time-resolved observations of water oxidation intermediates on a cobalt oxide nanoparticle catalyst. Nature chemistry, 2014. 6(4):p. 362.
[34] Surendranath, Y., M.W. Kanan, and D.G. Nocera, Mechanistic studies of the oxygen evolution reaction by a cobalt-phosphate catalyst at neutral pH. Journal of the American Chemical Society, 2010. 132(46): p. 16501-16509.

[35] Schalenbach, Maximilian, Geert Tjarks, Marcelo Carmo, Wiebke Lueke, Martin Mueller, and Detlef Stolten. "Acidic or alkaline? Towards a new perspective on the efficiency of water electrolysis." Journal of The Electrochemical Society 163, no. 11 (2016): F3197.

[36] Allebrod, Frank, Christodoulos Chatzichristodoulou, Pia Lolk Mollerup, and Mogens Bjerg Mogensen. "Electrical conductivity measurements of aqueous and immobilized potassium hydroxide." international journal of hydrogen energy 37, no. 21 (2012): 16505-16514.

[37] Kreuter, W., and H. Hofmann. "Electrolysis: the important energy transformer in a world of sustainable energy." International Journal of Hydrogen Energy 23, no. 8 (1998): 661-666.

[38] Olivares-RamÃ-rez, J. M., M. L. Campos-Cornelio, J. Uribe GodÃ-nez, E. Borja-Arco, and R. H. Castellanos. "Studies on the hydrogen evolution reaction on different stainless steels." International Journal of Hydrogen Energy 32, no. 15 (2007): 3170-3173.

[39] Bard, A. J., M. Stratmann, D. McDonald, and P. Schmuki. "Encyclopedia of Electrochemistry, vol. 5, Electrochemical Engineering." (2007): 161-223.

[40] Conway, B. E., and B. V. Tilak. "Interfacial processes involving electrocatalytic evolution and oxidation of H2, and the role of chemisorbed H." Electrochimica Acta 47, no. 22-23 (2002): 3571-3594.

[41] Laursen, Anders B., SÃ¿ren KegnÃes, SÃ¿ren Dahl, and Ib Chorkendorff. "Molybdenum sulfidesâATefficient and viable materials for electro-and photoelectrocatalytic hydrogen evolution." Energy and Environmental Science 5, no. 2 (2012): 5577-5591.

[42] Morales-Guio, Carlos G., Lucas-Alexandre Stern, and Xile Hu. "Nanostructured hydrotreating catalysts for electrochemical hydrogen evolution." Chemical Society Reviews 43, no. 18 (2014): 6555-6569.

[43] Fabbri, E., et al., Developments and perspectives of oxide-based catalysts for the oxygen evolution reaction. Catalysis Science and Technology, 2014. 4(11): p. 3800-3821.

[44] Matsumoto, Y., and E. Sato. "Electrocatalytic properties of transition metal oxides for oxygen evolution reaction." Materials chemistry and physics 14, no. 5 (1986): 397-426.

[45] Wang, Fengmei, Tofik Ahmed Shifa, Xueying Zhan, Yun Huang, Kaili Liu, Zhongzhou Cheng, Chao Jiang, and Jun He. "Recent advances in transitionmetal dichalcogenide based nanomaterials for water splitting." Nanoscale 7, no. 47 (2015): 19764-19788.

[46] Long, X., Li, J., Xiao, S., Yan, K., Wang, Z., Chen, H., & Yang, S. (2014). A strongly coupled graphene and FeNi double hydroxide hybrid as an excellent electrocatalyst for the oxygen evolution reaction. *Angewandte Chemie, 126*(29), 7714-7718.

[47] McCrory, C. C., Jung, S., Peters, J. C., & Jaramillo, T. F. (2013). Benchmarking heterogeneous electrocatalysts for the oxygen evolution reaction. *Journal of the American Chemical Society, 135*(45), 16977-16987.

[48] Wang, J., Zhang, T., Li, M., Yang, Y., Lu, P., Ning, P., & Wang, Q. (2018). Arsenic removal from water/wastewater using layered double hydroxide derived adsorbents, a critical review. *RSC advances, 8*(40), 22694-22709.

[49] Luo, J., Im, J.-H., Mayer, M. T., Schreier, M., Nazeeruddin, M. K., Park, N.-G., . . . Grätzel, M. (2014). Water photolysis at 12.3% efficiency via perovskite photovoltaics and Earth-abundant catalysts. *Science, 345*(6204), 1593-1596.

[50] Eliaz, N., & Gileadi, E. (2019). *Physical electrochemistry: fundamentals, techniques, and applications*: John Wiley & Sons.

[51] IEA, Global share of total energy supply by source, (2019), IEA, Paris.

[52] Hernández, W. Y., Lauwaert, J., Van Der Voort, P., & Verberckmoes, A. (2017). Recent advances on the utilization of layered double hydroxides (LDHs) and related heterogeneous catalysts in a lignocellulosic-feedstock biorefinery scheme. *Green Chemistry, 19*(22), 5269-5302.

[53] Lin, X., Li, R., Lu, M., Chen, C., Li, D., Zhan, Y., & Jiang, L. (2015). Carbon dioxide reforming of methane over Ni catalysts prepared from Ni–Mg–Al layered double hydroxides: Influence of Ni loadings. *Fuel, 162*, 271-280.

[54] Palacio, L. A., Velásquez, J., Echavarría, A., Faro, A., Ribeiro, F. R., & Ribeiro, M. F. (2010). Total oxidation of toluene over calcined trimetallic hydrotalcites type catalysts. *Journal of Hazardous Materials, 177*(1-3), 407-413.

[55] Ortega, K. F., Rein, D., Lüttmann, C., Heese, J., Özcan, F., Heidelmann, M., . . . Behrens, M. (2017). Ammonia decomposition and synthesis over multinary

magnesioferrites: promotional effect of Ga on Fe catalysts for the decomposition reaction. *Chem Cat Chem, 9*(4), 659-671.

[56] Balsamo, N., Mendieta, S., Oliva, M., Eimer, G., & Crivello, M. (2012). Synthesis and characterization of metal mixed oxides from layered double hydroxides. *Procedia Materials Science, 1*, 506-513.

[57] Li, S., Wang, H., Li, W., Wu, X., Tang, W., & Chen, Y. (2015). Effect of Cu substitution on promoted benzene oxidation over porous CuCo-based catalysts derived from layered double hydroxide with resistance of water vapor. *Applied Catalysis B: Environmental, 166*, 260-269.

[58] Indra, A., Menezes, P. W., Zaharieva, I., Baktash, E., Pfrommer, J., Schwarze, M., . . . Driess, M. (2013). Active mixed-valent MnOx water oxidation catalysts through partial oxidation (corrosion) of nanostructured MnO particles. *Angewandte Chemie International Edition, 52*(50), 13206-13210.

[59] Rausch, B., Symes, M. D., Chisholm, G., & Cronin, L. (2014). Decoupled catalytic hydrogen evolution from a molecular metal oxide redox mediator in water splitting. *Science, 345*(6202), 1326-1330.

[60] Wang, X., Yu, L., Guan, B. Y., Song, S., & Lou, X. W. (2018). Metal–organic framework hybrid-assisted formation of Co3O4/Co-Fe oxide double-shelled nanoboxes for enhanced oxygen evolution. *Advanced materials, 30*(29), 1801211.

[61] Gao, R., & Yan, D. (2020). Recent development of Ni/Fe-based micro/nanostructures toward photo/electrochemical water oxidation. *Advanced Energy Materials, 10*(11), 1900954.

[62] Tee, S. Y., Win, K. Y., Teo, W. S., Koh, L. D., Liu, S., Teng, C. P., & Han, M. Y. (2017). Recent progress in energy-driven water splitting. *Advanced science, 4*(5), 1600337.

[63] Konieczny, A., Mondal, K., Wiltowski, T., & Dydo, P. (2008). Catalyst development for thermocatalytic decomposition of methane to hydrogen. *International Journal of Hydrogen Energy, 33*(1), 264-272.

[64] Turner, J., Sverdrup, G., Mann, M. K., Maness, P. C., Kroposki, B., Ghirardi, M., . . . Blake, D. (2008). Renewable hydrogen production. *International journal of energy research, 32*(5), 379-407.

[65] Wang, P., Zhang, X., Zhang, J., Wan, S., Guo, S., Lu, G., . . . Huang, X. (2017). Precise tuning in platinum-nickel/nickel sulfide interface nanowires for synergistic hydrogen evolution catalysis. *Nature communications, 8*(1), 1-9.

[66] Lim, J., Park, D., Jeon, S. S., Roh, C. W., Choi, J., Yoon, D., . . . Lee, H. (2018). Ultrathin IrO2 nanoneedles for electrochemical water oxidation. *Advanced Functional Materials, 28*(4), 1704796.

[67] Zhao, G., Rui, K., Dou, S. X., & Sun, W. (2018). Heterostructures for electrochemical hydrogen evolution reaction: a review. *Advanced Functional Materials, 28*(43), 1803291.

[68] Carmo, M., Fritz, D. L., Mergel, J., & Stolten, D. (2013). A comprehensive review on PEM water electrolysis. *International Journal of Hydrogen Energy, 38*(12), 4901-4934.

[69] Roger, I., Shipman, M. A., & Symes, M. D. (2017). Earth-abundant catalysts for electrochemical and photoelectrochemical water splitting. *Nature Reviews Chemistry, 1*(1), 1-13.

[70] Crabtree, G., Dresselhaus, M., & Buchanan, M. (2004). Storing Hydrogen. *Phys. Today, 57*, 39-45.

[71] Kreuter, W., & Hofmann, H. (1998). Electrolysis: the important energy transformer in a world of sustainable energy. *International Journal of Hydrogen Energy, 23*(8), 661-666.

[72] Shi, Y., & Zhang, B. (2016). Recent advances in transition metal phosphide nanomaterials: synthesis and applications in hydrogen evolution reaction. *Chemical Society Reviews, 45*(6), 1529-1541.

[73] Ying, J., Jiang, G., Cano, Z. P., Han, L., Yang, X.-Y., & Chen, Z. (2017). Nitrogen-doped hollow porous carbon polyhedrons embedded with highly dispersed Pt nanoparticles as a highly efficient and stable hydrogen evolution electrocatalyst. *Nano Energy, 40*, 88-94.

[74] Fan, H., Yu, H., Zhang, Y., Zheng, Y., Luo, Y., Dai, Z., . . . Yan, Q. (2017). Fe-doped Ni3C nanodots in N-doped carbon nanosheets for efficient hydrogen-evolution and oxygen-evolution electrocatalysis. *Angewandte Chemie International Edition, 56*(41), 12566-12570.

[75] Kim, Y., Jackson, D. H., Lee, D., Choi, M., Kim, T. W., Jeong, S. Y., . . . Chang, H. (2017). In situ electrochemical activation of atomic layer deposition coated MoS2 basal planes for efficient hydrogen evolution reaction. *Advanced Functional Materials, 27*(34), 1701825.

[76] Binz, C., Gosens, J., Hansen, T., & Hansen, U. E. (2017). Toward technology-sensitive catching-up policies: insights from renewable energy in China. *World Development, 96*, 418-437.

[77] Schlapbach, L., Züttel, A., Gröning, P., Gröning, O., & Aebi, P. (2001). Hydrogen for novel materials and devices. *Applied Physics A, 72*(2), 245-253.

[78] McCrory, C. C., Jung, S., Ferrer, I. M., Chatman, S. M., Peters, J. C., & Jaramillo, T. F. (2015). Benchmarking hydrogen evolving reaction and oxygen evolving reaction electrocatalysts for solar water splitting devices. *Journal of the American Chemical Society, 137*(13), 4347-4357.

[79] Carmo, M., Fritz, D. L., Mergel, J., & Stolten, D. (2013). A comprehensive review on PEM water electrolysis. *International Journal of Hydrogen Energy, 38*(12), 4901-4934.

[80] Grimes, C. A., Varghese, O. K., & Ranjan, S. (2008). *Light, water, hydrogen: the solar generation of hydrogen by water photoelectrolysis* (Vol. 546): Springer.

[81] Kibsgaard, J., Jaramillo, T. F., & Besenbacher, F. (2014). Building an appropriate active-site motif into a hydrogen-evolution catalyst with thiomolybdate [Mo3S13] 2− clusters. *Nature chemistry, 6*(3), 248-253.

[82] Yan, Y., Ge, X., Liu, Z., Wang, J.-Y., Lee, J.-M., & Wang, X. (2013). Facile synthesis of low crystalline MoS 2 nanosheet-coated CNTs for enhanced hydrogen evolution reaction. *Nanoscale, 5*(17), 7768-7771.

[83] Chu, S., & Majumdar, A. (2012). Opportunities and challenges for a sustainable energy future. *Nature, 488*(7411), 294-303.

[84] Mukherjee, D., Austeria, P., & Sampath, S. (2017). ACS Energy Lett. 2016, 1, 367; b) B. *Konkena, J. Masa, AJR Botz, I. Sinev, W. Xia, J. Koßmann, R. Drautz, M. Muhler, W. Schuhmann, ACS Catal, 7,* 229.

[85] Zhang, J., Zhao, L., Liu, A., Li, X., Wu, H., & Lu, C. (2015). Three-dimensional MoS2/rGO hydrogel with extremely high double-layer capacitance as active catalyst for hydrogen evolution reaction. *Electrochimica Acta, 182*, 652-658.

[86] Deng, J., Ren, P., Deng, D., & Bao, X. (2015). Enhanced electron penetration through an ultrathin graphene layer for highly efficient catalysis of the hydrogen evolution reaction. *Angewandte Chemie International Edition, 54*(7), 2100-2104.

[87] Tang, H., Dou, K., Kaun, C.-C., Kuang, Q., & Yang, S. (2014). MoSe 2 nanosheets and their graphene hybrids: synthesis, characterization and hydrogen evolution reaction studies. *Journal of materials chemistry a, 2*(2), 360-364.

[88] Ledendecker, M., Clavel, G., Antonietti, M., & Shalom, M. (2015). Highly porous materials as tunable electrocatalysts for the hydrogen and oxygen evolution reaction. *Advanced Functional Materials, 25*(3), 393-399.

[89] Zhou, X., Gan, Y., Du, J., Tian, D., Zhang, R., Yang, C., & Dai, Z. (2013). A review of hollow Pt-based nanocatalysts applied in proton exchange membrane fuel cells. *Journal of Power Sources, 232*, 310-322.

[90] Walter, M. G., Warren, E. L., McKone, J. R., Boettcher, S. W., Mi, Q., Santori, E. A., & Lewis, N. S. (2010). Solar water splitting cells. *Chemical reviews, 110*(11), 6446-6473.

[91] Subbaraman, R., Tripkovic, D., Strmcnik, D., Chang, K.-C., Uchimura, M., Paulikas, A. P., Markovic, N. M. (2011). Enhancing hydrogen evolution activity in water splitting by tailoring Li+-Ni (OH) 2-Pt interfaces. *Science, 334*(6060), 1256-1260.

[92] Subbaraman, R., Tripkovic, D., Chang, K.-C., Strmcnik, D., Paulikas, A. P., Hirunsit, P, Markovic, N. M. (2012). Trends in activity for the water electrolyser reactions on 3d M (Ni, Co, Fe, Mn) hydr (oxy) oxide catalysts. *Nature materials, 11*(6), 550-557.

[93] Zhang, P., Zhang, J., & Gong, J. (2014). Tantalum-based semiconductors for solar water splitting. *Chemical Society Reviews, 43*(13), 4395-4422.

[94] Lasia, A. (2010). Hydrogen evolution reaction. *Handbook of fuel cells, 815*.

[95] Danilovic, N., Subbaraman, R., Strmcnik, D., Stamenkovic, V., & Markovic, N. (2013). Electrocatalysis of the HER in acid and alkaline media. *Journal of the Serbian Chemical Society, 78*(12).

[96] Zeng, K., & Zhang, D. (2010). Recent progress in alkaline water electrolysis for hydrogen production and applications. *Progress in energy and combustion science, 36*(3), 307-326.

[97] Greeley, J., Jaramillo, T. F., Bonde, J., Chorkendorff, I., & Nørskov, J. K. (2006). Computational high-throughput screening of electrocatalytic materials for hydrogen evolution. *Nature materials, 5*(11), 909-913.

[98] Wang, H., Lee, H.-W., Deng, Y., Lu, Z., Hsu, P.-C., Liu, Y., . . . Cui, Y. (2015). Bifunctional non-noble metal oxide nanoparticle electrocatalysts through lithium-induced conversion for overall water splitting. *Nature communications, 6*(1), 1-8.

[99] Gong, M., & Dai, H. (2015). A mini review of NiFe-based materials as highly active oxygen evolution reaction electrocatalysts. *Nano Research, 8*(1), 23-39.

[100] Song, F., & Hu, X. (2014). Exfoliation of layered double hydroxides for enhanced oxygen evolution catalysis. *Nature communications, 5*(1), 1-9.

[101] Sheng, W., Gasteiger, H. A., & Shao-Horn, Y. (2010). Hydrogen oxidation and evolution reaction kinetics on platinum: acid vs alkaline electrolytes. *Journal of The Electrochemical Society, 157*(11), B1529.

[102] Campbell, J., & Whiteker, R. (1969). A periodic table based on potential-pH diagrams. *Journal of Chemical Education, 46*(2), 90.

[103] Luo, J., Im, J.-H., Mayer, M. T., Schreier, M., Nazeeruddin, M. K., Park, N.-G., Grätzel, M. (2014). Water photolysis at 12.3% efficiency via perovskite photovoltaics and Earth-abundant catalysts. *Science, 345*(6204), 1593-1596.

[104] Ray, C., Lee, S. C., Jin, B., Kundu, A., Park, J. H., & Jun, S. C. (2018). Stacked porous iron-doped nickel cobalt phosphide nanoparticle: an efficient and stable water splitting electrocatalyst. *ACS sustainable chemistry & engineering, 6*(5), 6146-6156.

[105] Assunção, N. A., De Giz, M., Tremiliosi-Filho, G., & Gonzalez, E. R. (1997). A study of the hydrogen evolution reaction on a Ni/NiFeS electrodeposited coating. *Journal of The Electrochemical Society, 144*(8), 2794.

[106] Gu, Y., Chen, S., Ren, J., Jia, Y. A., Chen, C., Komarneni, S., . . . Yao, X. (2018). Electronic structure tuning in Ni3FeN/r-GO aerogel toward bifunctional electrocatalyst for overall water splitting. *Acs Nano, 12*(1), 245-253.

[107] Xing, J., Li, H., Cheng, M. M.-C., Geyer, S. M., & Ng, K. S. (2016). Electro-synthesis of 3D porous hierarchical Ni–Fe phosphate film/Ni foam as a high-efficiency bifunctional electrocatalyst for overall water splitting. *Journal of materials chemistry a, 4*(36), 13866-13873.

[108] Xiao, C., Zhang, B., & Li, D. (2017). Partial-sacrificial-template synthesis of Fe/Ni phosphides on Ni foam: a strongly stabilized and efficient catalyst for electrochemical water splitting. *Electrochimica Acta, 242*, 260-267.

[109] Hu, J., Ou, Y., Li, Y., Gao, D., Zhang, Y., & Xiao, P. (2018). FeCo2S4 nanosheet arrays supported on Ni foam: an efficient and durable bifunctional electrocatalyst for overall water-splitting. *ACS sustainable chemistry & engineering, 6*(9), 11724-11733.

[110] Chen, Z.-J., Cao, G.-X., Gan, L.-Y., Dai, H., Xu, N., Zang, M.-J., Wang, P. (2018). Highly dispersed platinum on honeycomb-like NiO@ Ni film as a synergistic electrocatalyst for the hydrogen evolution reaction. *Acs Catalysis, 8*(9), 8866-8872.

[111] Zhou, L., Shao, M., Li, J., Jiang, S., Wei, M., & Duan, X. (2017). Two-dimensional ultrathin arrays of CoP: electronic modulation toward high performance overall water splitting. *Nano Energy, 41*, 583-590.

[112] Liu, B., Zhao, Y. F., Peng, H. Q., Zhang, Z. Y., Sit, C. K., Yuen, M. F., . . . Zhang, W. J. (2017). Nickel–cobalt diselenide 3D mesoporous nanosheet networks supported on Ni foam: an all-pH highly efficient integrated electrocatalyst for hydrogen evolution. *Advanced materials, 29*(19), 1606521.

[113] Zhang, W., Zou, Y., Liu, H., Chen, S., Wang, X., Zhang, H., . . . Yang, D. (2019). Single-crystalline (FexNi1-x) 2P nanosheets with dominant {$011^{\bar{}}$ $1^{\bar{}}$} facets: Efficient electrocatalysts for hydrogen evolution reaction at all pH values. *Nano Energy, 56*, 813-822.

[114] Wan, J., Ye, W., Gao, R., Fang, X., Guo, Z., Lu, Y., & Yan, D. (2019). Synthesis from a layered double hydroxide precursor for a highly efficient oxygen evolution reaction. *Inorganic Chemistry Frontiers, 6*(7), 1793-1798.

[115] Arif, M., Yasin, G., Shakeel, M., Fang, X., Gao, R., Ji, S., & Yan, D. (2018). Coupling of bifunctional CoMn-layered double hydroxide@ graphitic C3N4 nanohybrids towards efficient photoelectrochemical overall water splitting. *Chemistry–An Asian Journal, 13*(8), 1045-1052.

[116] Friebel, D., Louie, M. W., Bajdich, M., Sanwald, K. E., Cai, Y., Wise, A. M., . . . Alonso-Mori, R. (2015). Identification of highly active Fe sites in (Ni, Fe) OOH for electrocatalytic water splitting. *Journal of the American Chemical Society, 137*(3), 1305-1313.

[117] Gao, R., & Yan, D. (2020). Recent development of Ni/Fe-based micro/nanostructures toward photo/electrochemical water oxidation. *Advanced Energy Materials, 10*(11), 1900954.

[118] Long, X., Wang, Z., Xiao, S., An, Y., & Yang, S. (2016). Transition metal based layered double hydroxides tailored for energy conversion and storage. *Materials today, 19*(4), 213-226.

[119] Jia, Y., Zhang, L., Gao, G., Chen, H., Wang, B., Zhou, J., . . . Qian, G. (2017). A heterostructure coupling of exfoliated Ni–Fe hydroxide nanosheet and defective graphene as a bifunctional electrocatalyst for overall water splitting. *Advanced materials, 29*(17), 1700017.

[120] Chen, G., Wang, T., Zhang, J., Liu, P., Sun, H., Zhuang, X., . . . Feng, X. (2018). Accelerated hydrogen evolution kinetics on NiFe-layered double hydroxide electrocatalysts by tailoring water dissociation active sites. *Advanced materials, 30*(10), 1706279.

[121] Chen, Q.-Q., Hou, C.-C., Wang, C.-J., Yang, X., Shi, R., & Chen, Y. (2018). Ir 4+-Doped NiFe LDH to expedite hydrogen evolution kinetics as a Pt-like electrocatalyst for water splitting. *Chemical Communications, 54*(49), 6400-6403.

[122] Tang, Y., Liu, Q., Dong, L., Wu, H. B., & Yu, X.-Y. (2020). Activating the hydrogen evolution and overall water splitting performance of NiFe LDH by cation doping and plasma reduction. *Applied Catalysis B: Environmental, 266*, 118627.

[123] Occelli, M. L., & Robson, H. (2012). *Expanded clays and other microporous solids*: Springer Science & Business Media.

[124] Cavani, F., Trifiro, F., & Vaccari, A. (1991). Hydrotalcite-type anionic clays: Preparation, properties and applications. *Catalysis today, 11*(2), 173-301.

[125] Kloprogge, J. T., Hickey, L., Trujillano, R., Holgado, M. J., San Román, M., Rives, V., Frost, R. L. (2006). Characterization of intercalated Ni/Al hydrotalcites prepared by the partial decomposition of urea. *Crystal growth & design, 6*(6), 1533-1536.

[126] Chibwe, K., & Jones, W. (1989). Intercalation of organic and inorganic anions into layered double hydroxides. *Journal of the Chemical Society, Chemical Communications* (14), 926-927.

[127] Naseem, S., Gevers, B., Boldt, R., Labuschagné, F. J. W., & Leuteritz, A. (2019). Comparison of transition metal (Fe, Co, Ni, Cu, and Zn) containing tri-metal layered double hydroxides (LDHs) prepared by urea hydrolysis. *RSC advances, 9*(6), 3030-3040.

[128] Han, Y., Liu, Z.-H., Yang, Z., Wang, Z., Tang, X., Wang, T., . . . Ooi, K. (2008). Preparation of Ni2+− Fe3+ layered double hydroxide material with high crystallinity and well-defined hexagonal shapes. *Chemistry of Materials, 20*(2), 360-363.

[129] Xu, Z. P., & Lu, G. Q. (2005). Hydrothermal synthesis of layered double hydroxides (LDHs) from mixed MgO and Al2O3: LDH formation mechanism. *Chemistry of Materials, 17*(5), 1055-1062.

[130] Wang, F., Wang, T., Sun, S., Xu, Y., Yu, R., & Li, H. (2018). One-step synthesis of Nickle Iron-layered double hydroxide/reduced graphene oxide/carbon nanofibres composite as electrode materials for asymmetric supercapacitor. *Scientific reports, 8*(1), 1-10.

[131] Xu, Z. P., Stevenson, G. S., Lu, C.-Q., Lu, G. Q., Bartlett, P. F., & Gray, P. P. (2006). Stable suspension of layered double hydroxide nanoparticles in aqueous solution. *Journal of the American Chemical Society, 128*(1), 36-37.

[132] Zhao, Y., Li, F., Zhang, R., Evans, D. G., & Duan, X. (2002). Preparation of layered double-hydroxide nanomaterials with a uniform crystallite size using a new method involving separate nucleation and aging steps. *Chemistry of Materials, 14*(10), 4286-4291.

[133] Dong, H., Chen, M., Rahman, S., Parekh, H. S., Cooper, H. M., & Xu, Z. P. (2014). Engineering small MgAl-layered double hydroxide nanoparticles for enhanced gene delivery. *Applied clay science, 100*, 66-75.

[134] Prince, J., Montoya, A., Ferrat, G., & Valente, J. S. (2009). Proposed general sol− gel method to prepare multimetallic layered double hydroxides: synthesis, characterization, and envisaged application. *Chemistry of Materials, 21*(24), 5826-5835.

[135] Prevot, V., Forano, C., & Besse, J. (2005). Hydrolysis in polyol: new route for hybrid-layered double hydroxides preparation. *Chemistry of Materials, 17*(26), 6695-6701.

[136] Prinetto, F., Ghiotti, G., Graffin, P., & Tichit, D. (2000). Synthesis and characterization of sol–gel Mg/Al and Ni/Al layered double hydroxides and comparison with co-precipitated samples. *Microporous and Mesoporous Materials*, *39*(1-2), 229-247.

[137] Aramendía, M. a. A., Borau, V., Jiménez, C., Marinas, J. M., Ruiz, J. R., & Urbano, F. J. (2002). Comparative study of Mg/M (III)(M= Al, Ga, In) layered double hydroxides obtained by coprecipitation and the sol–gel method. *Journal of solid state chemistry, 168*(1), 156-161.

[138] Tichit, D., Lorret, O., Coq, B., Prinetto, F., & Ghiotti, G. (2005). Synthesis and characterization of Zn/Al and Pt/Zn/Al layered double hydroxides obtained by the sol–gel method. *Microporous and Mesoporous Materials*, *80*(1-3), 213-220.

[139] Hu, G., Wang, N., O'Hare, D., & Davis, J. (2007). Synthesis of magnesium aluminium layered double hydroxides in reverse microemulsions. *Journal of Materials Chemistry*, *17*(21), 2257-2266.

[140] Bellezza, F., Nocchetti, M., Posati, T., Giovagnoli, S., & Cipiciani, A. (2012). Synthesis of colloidal dispersions of NiAl, ZnAl, NiCr, ZnCr, NiFe, and MgFe hydrotalcite-like nanoparticles. *Journal of colloid and interface science*, *376*(1), 20-27.

[141] Bellezza, F., Cipiciani, A., Costantino, U., Nocchetti, M., & Posati, T. (2009). Hydrotalcite-Like Nanocrystals from Water-in-Oil Microemulsions: Wiley Online Library.

[142] Guo, X., Zhang, F., Evans, D. G., & Duan, X. (2010). Layered double hydroxide films: synthesis, properties and applications. *Chemical Communications*, *46*(29), 5197-5210.

[143] Shao, M., Han, J., Shi, W., Wei, M., & Duan, X. (2010). Layer-by-layer assembly of porphyrin/layered double hydroxide ultrathin film and its electrocatalytic behavior for H2O2. *Electrochemistry communications, 12*(8), 1077-1080.

[144] Liu, Z., Ma, R., Osada, M., Iyi, N., Ebina, Y., Takada, K., & Sasaki, T. (2006). Synthesis, anion exchange, and delamination of Co− Al layered double hydroxide: assembly of the exfoliated nanosheet/polyanion composite films and magneto-optical studies. *Journal of the American Chemical Society*, *128*(14), 4872-4880.

[145] Indira, P. (1994). Electrogeneration of base by cathodic reduction of anions: novel one-step route to unary and layered double hydroxides (LDHs). *Journal of Materials Chemistry*, *4*(9), 1487-1490.

[146] Scavetta, E., Mignani, A., Prandstraller, D., & Tonelli, D. (2007). Electrosynthesis of thin films of Ni, Al hydrotalcite like compounds. *Chemistry of Materials*, *19*(18), 4523-4529.

[147] Vlamidis, Y., Scavetta, E., Gazzano, M., & Tonelli, D. (2016). Iron vs aluminum based layered double hydroxides as water splitting catalysts. *Electrochimica Acta*, *188*, 653-660.

[148] Basile, F., Benito, P., Fornasari, G., Monti, M., Scavetta, E., Tonelli, D., & Vaccari, A. (2010). Novel Rh-based structured catalysts for the catalytic partial oxidation of methane. *Catalysis today*, *157*(1-4), 183-190.

[149] Li, X., Zhou, J., Li, X., Xin, M., Cai, T., Xing, W., . . . Yan, Z. (2017). Bifuntional petaloid nickel manganese layered double hydroxides decorated on a freestanding carbon foam for flexible asymmetric supercapacitor and oxygen evolution. *Electrochimica Acta*, *252*, 275-285.

[150] Chen, L., Zhang, H., Chen, L., Wei, X., Shi, J., & He, M. (2017). Facile synthesis of Cu doped cobalt hydroxide (Cu–Co (OH) 2) nano-sheets for efficient electrocatalytic oxygen evolution. *Journal of materials chemistry a*, *5*(43), 22568-22575.

[151] Li, D., Hao, G., Guo, W., Liu, G., Li, J., & Zhao, Q. (2020). Highly efficient Ni nanotube arrays and Ni nanotube arrays coupled with NiFe layered-double-hydroxide electrocatalysts for overall water splitting. *Journal of Power Sources*, *448*, 227434.

[152] N.K. Chaudhari, H. Jin, B. Kim, K. Lee, Nanoscale 9 (2017) 12231–12247

[153] J.L. He, B.B. Hu, Y. Zhao, Adv. Funct. Mater. 26 (2016) 5998–6004.

[154] N.K. Chaudhari, S. Chaudhari, J.S. Yu, Chemsuschem 7 (2014) 3102–3111. 768

[155] N.K. Chaudhari, M.S. Kim, T.S. Bae, J.S. Yu, Electrochim. Acta (2013) 60–67.

[156] X.J. Chen, G.F. Zeng, T.T. Gao, Z.Y. Jin, Y.J. Zhang, H.Y. Yuan, D. Xiao, Electrochem. Commun. 74 (2017) 42–47.

[157] C.C. Du, M.X. Shang, J.X. Mao, W.B. Song, J. Mater. Chem. A 5 (2017) 15940–15949. 809

[158] J.Z. Li, G.D. Wei, Y.K. Zhu, Y.L. Xi, X.X. Pan, Y. Ji, I.V. Zatovsky, W. Han, J. Mater. Chem. A 5 (2017) 14828–14837. 811

[159] L. Yang, Z.L. Guo, J. Huang, Y.N. Xi, R.J. Gao, G. Su, W. Wang, L.X. Cao, B.H. Dong, Adv. Mater. 29 (2017) 1704574.

[160] M. Blasco-Ahicart, J. Soriano-Lopez, J.R. Galan-Mascaros, Chemelectrochem 4 (2017) 3296–3301. 791

[161] T. Butburee, Y. Bai, H.J. Wang, H.J. Chen, Z.L. Wang, G. Liu, J. Zou, P. Khemthong, G.Q.M. Lu, L.Z. Wang, Adv. Mater. 30 (2018) 1705666. 793

[162] G.M. Wang, H.Y. Wang, Y.C. Ling, Y.C. Tang, X.Y. Yang, R.C. Fitzmorris, C.C. Wang, J.Z. Zhang, Y. Li, Nano Lett. 11 (2011) 3026–3033. 795

[163] Z.W. Wang, X.L. Li, H. Ling, C.K. Tan, L.P. Yeo, A.C. Grimsdale, A.I.Y. Tok, Small 14 (2018) 1800395.

[164] Y.P. Liu, X. Liang, L. Gu, Y. Zhang, G.D. Li, X.X. Zou, J.S. Chen, Nat. Commun. 9 (2018) 2609.

[165] Y.P. Liu, X. Liang, L. Gu, Y. Zhang, G.D. Li, X.X. Zou, J.S. Chen, Nat. Commun. 9 (2018) 2609.

[166] X. Liu, B. You, Y.J. Sun, ACS Sustain. Chem. Eng. 5 (2017) 4778–4784

[167] H.Y. Li, S.M. Chen, X.F. Jia, B. Xu, H.F. Lin, H.Z. Yang, L. Song, X. Wang, Nat. Commun. 8 (2017) 15377

[168] L. Zhou, M.F. Shao, M. Wei, X. Duan, J. Energy Chem. 26 (2017) 1094–1106.

[169] L. Zhou, M.F. Shao, C. Zhang, J.W. Zhao, S. He, D.M. Rao, M. Wei, D.G. Evans, X. Duan, Adv. Mater. 29 (2017) 1604080

[170] M.Y. Gao, C. Yang, Q.B. Zhang, J.R. Zeng, X.T. Li, Y.X. Hua, C.Y. Xu, P. Dong, J. Mater. Chem. A 5 (2017) 5797–5805.

[171] X. Gao, J. Li, R. Du, J.Y. Zhou, M.Y. Huang, R. Liu, J. Li, Z.Q. Xie, L.Z. Wu, Z.F. Liu, J. Zhang, Adv. Mater. 29 (2017) 1605308.

[172] N. Jiang, B. You, M.L. Sheng, Y.J. Sun, Angew. Chem. Int. Ed. 54 (2015) 6251–6254.

[173] N. Jiang, B. You, M.L. Sheng, Y.J. Sun, Chemcatchem 8 (2016) 106–112.

[174] Y.J. Chen, Z.Y. Ren, H.Y. Fu, X. Zhang, G.H. Tian, H.G. Fu, Small 14 (2018) 1800763. [175] S.C. Du, Z.Y. Ren, J. Zhang, J. Wu, W. Xi, J.Q. Zhu, H.G. Fu, Chem. Commun. 51 (2015) 8066–8069.

[176] C. Hang, J. Zhang, J.W. Zhu, W.Q. Li, Z.K. Kou, Y.H. Huang, Adv. Energy. Mater. 8 (2018) 1703539.

[177] J. Mathias, "How Does FTIR Work_ _ Innovatech Labs." 2015.

[178] C. Sophia and J. M. Gohil, "Chapter 19 - Microbial Desalination Cell Technology: Functions and Future Prospects," P. P. Kundu and K. B. T.-P. and R. T. in M. F. C. Dutta, Eds. Elsevier, 2018, pp. 399–422.

[179] Voiry, D., Chhowalla, M., Gogotsi, Y., Kotov, N. A., Li, Y., Penner, R. M., . . . Weiss, P. S. (2018). Best practices for reporting electrocatalytic performance of nanomaterials (Vol. 12, pp. 9635-9638): ACS Publications.

[180] Liu, J., Zheng, Y., Wang, Z., Lu, Z., Vasileff, A., & Qiao, S.-Z. (2018). Free-standing single-crystalline NiFe-hydroxide nanoflake arrays: a self-activated and robust electrocatalyst for oxygen evolution. *Chemical Communications, 54*(5), 463-466.

[181] Li, H., Zhao, X., Liu, H., Chen, S., Yang, X., Lv, C., . . . Yang, D. (2018). Sub-1.5 nm Ultrathin CoP Nanosheet Aerogel: Efficient Electrocatalyst for Hydrogen Evolution Reaction at All pH Values. *Small, 14*(41), 1802824.

[182] L. Li, R. Ma, Y. Ebina, K. Fukuda, K. Takada, T. Sasaki, J. Am. Chem. Soc. 129 (2007) 8000-8007.

[183] Lee, Y., Choi, J. H., Jeon, H. J., Choi, K. M., Lee, J. W., & Kang, J. K. (2011). Titanium-embedded layered double hydroxides as highly efficient water oxidation photocatalysts under visible light. *Energy & Environmental Science, 4*(3), 914-920.

[184] Y. Gogotsi and R. M. Penner, "Energy Storage in Nanomaterials – Capacitive, Pseudocapacitive, or Battery-like," *ACS Nano*, vol. 12, no. 3, pp. 2081–2083, Mar. (2018)